Title: **Cortico-Fugal Regulation of Predictive Coding.**

Authors: Alexandria M.H. Lesicko[1], Christopher F. Angeloni[2], Jennifer M. Blackwell[3], Mariella De Biasi[4,5,6], Maria N. Geffen[1,6,7]

Affiliations:

1. Department of Otorhinolaryngology, University of Pennsylvania, Philadelphia, United States
2. Department of Psychology, University of Pennsylvania, Philadelphia, United States
3. Department of Neurobiology and Behavior, Stony Brook University, Stony Brook, New York, United States
4. Department of Psychiatry, University of Pennsylvania, Philadelphia, United States
5. Department of Systems Pharmacology and Experimental Therapeutics, University of Pennsylvania, Philadelphia, United States
6. Department of Neuroscience, University of Pennsylvania, Philadelphia, United States
7. Department of Neurology, University of Pennsylvania, Philadelphia, United States

Corresponding author: Dr. Maria N. Geffen
Stemmler Hall G10
3450 Hamilton Walk
Philadelphia, PA 19104
(215)898-0872
mgeffen@pennmedicine.upenn.edu

Keywords: prediction error, hierarchical predictive coding, inferior colliculus, auditory cortex, cortico-collicular, stimulus specific adaptation, deviance detection

ABSTRACT

Sensory systems must account for both contextual factors and prior experience to adaptively engage with the dynamic external environment. In the central auditory system, neurons modulate their responses to sounds based on statistical context. These response modulations can be understood through a hierarchical predictive coding lens: responses to repeated stimuli are progressively decreased, in a process known as repetition suppression, whereas unexpected stimuli produce a prediction error signal. Prediction error incrementally increases along the auditory hierarchy from the inferior colliculus (IC) to the auditory cortex (AC), suggesting that these regions may engage in hierarchical predictive coding. A potential substrate for top-down predictive cues is the massive set of descending projections from the auditory cortex to subcortical structures. To assess the role of these projections in predictive coding, we optogenetically suppressed the auditory cortico-collicular feedback in awake mice while recording responses from IC neurons to stimuli designed to test prediction error and repetition suppression. Suppression of the cortico-collicular pathway led to a decrease in prediction error in IC. Repetition suppression was unaffected by cortico-collicular inactivation, suggesting that this metric may reflect fatigue of bottom-up sensory inputs rather than predictive processing. We also discovered populations of IC neurons that exhibit repetition enhancement, an increase in firing with stimulus repetition, and error suppression, a stronger response to a tone in a predictable rather than unpredictable context. Cortico-collicular suppression led to a decrease in repetition enhancement in the central nucleus and a reduction in error suppression in shell regions of IC. These changes in predictive coding metrics arose from bidirectional modulations in the response to the standard and deviant contexts, such that neurons in IC responded more similarly to each context in the absence of cortical input. Our results demonstrate that the auditory cortex provides cues about the statistical context of sound to subcortical brain regions via direct feedback, regulating processing of both prediction and repetition.

INTRODUCTION

Sensory systems differentially encode environmental stimuli depending on the context in which they are encountered (De Franceschi & Barkat, 2020; Herrmann et al., 2015; Jaramillo et al., 2014; Pakan et al., 2016; Takesian et al., 2018; Zhai et al., 2020). The same physical stimulus can elicit distinct neuronal responses depending on whether it is predictable or unexpected in a given sensory stream (Weissbart et al., 2020; Yaron et al., 2012). One framework for understanding this dynamic sensory capability is hierarchical predictive coding, which suggests that neuronal networks form predictions about incoming stimuli based on the statistics of prior experience (Friston & Kiebel, 2009). These predictions are generated at higher levels of the sensory hierarchy and broadcast to lower stations to minimize processing of redundant input and maximize coding efficiency (Friston, 2009; Friston & Kiebel, 2009). Any mismatch between predictions and representations of sensory input is coded in a neuronal response known as a "prediction error", which is further propagated up the sensory hierarchy, ultimately allowing for the formation of updated predictions (Friston & Kiebel, 2009; Shipp, 2016). Multiple sensory modalities exhibit hierarchical predictive coding, including the motor, visual, and auditory systems (Okada et al., 2018; Parras et al., 2017; Rao & Ballard, 1999; Rauss et al., 2011; Schellekens et al., 2016; Shipp et al., 2013).

Neurons in select regions of the central auditory system are sensitive to statistical context, responding more strongly to a tone when it is presented rarely (a "deviant") than when it is commonplace (a "standard") (Ulanovsky et al., 2003). This phenomenon, known as stimulus specific adaptation (SSA), is prevalent in the auditory cortex (Natan et al., 2015; Ulanovsky et al., 2003). Weaker SSA is present in regions peripheral to the AC, including the auditory midbrain, or inferior colliculus (IC), and the auditory thalamus, or medial geniculate body (MGB) (Anderson et al., 2009; Antunes et al., 2010; Duque & Malmierca, 2015; Malmierca et al., 2009; Taaseh et al., 2011; Ulanovsky et al., 2003). Subdivisions in IC and MGB that receive descending projections from AC exhibit relatively higher SSA levels than their lemniscal counterparts (Antunes et al., 2010; Duque et al., 2012), suggesting that SSA may be generated de novo in AC and subsequently broadcast to subcortical structures via cortico-fugal projections (Nelken & Ulanovsky, 2007). However, silencing of AC through cooling leads to modulation, but not abolishment, of SSA in IC and MGB of anesthetized rats (Anderson & Malmierca, 2013; Antunes & Malmierca, 2011), indicating that SSA is at least partially produced in subcortical structures.

SSA comprises two distinct underlying processes: repetition suppression and prediction error (Harms et al., 2014; Parras et al., 2017; Ruhnau et al., 2012). Repetition suppression is characterized by a decrease in firing rate to each subsequent presentation of a standard tone (Auksztulewicz &

Friston, 2016; Parras et al., 2017). Prediction error is thought to signal the mismatch between the predicted input, based on prior experience with repeated presentations of the standard, and the actual sensory input when a deviant tone is presented (Friston, 2009; Friston & Kiebel, 2009). Whereas repetition suppression is thought to potentially reflect synaptic depression, prediction error has been proposed to underlie deviance detection (Parras et al., 2017; Taaseh et al., 2011). Prediction error increases along the auditory hierarchy and is more prevalent in regions of IC and MGB that receive cortical feedback (Parras et al., 2017), suggesting that these subcortical regions may engage in hierarchical predictive coding, with AC potentially providing predictive cues to IC and MGB.

Virtually all models of hierarchical predictive coding to date have focused on intra-cortical connections, with the massive system of descending cortico-fugal projections remaining unexplored (Asilador & Llano, 2020; Bastos et al., 2012). Here, we investigated how inputs from AC to IC, the first station in the auditory system in which prediction error is found, shape metrics associated with predictive coding and deviance detection (Parras et al., 2017). To test this, we optogenetically suppressed cortico-collicular feedback while recording neuronal responses in IC and found that metrics of both repetition and prediction in IC are altered in the absence of cortical input. Our results suggest that the cortico-collicular pathway sends cues from AC to IC regarding the statistical context of auditory stimuli.

105 METHODS

106 *Animals*

107 We performed experiments in six adult Cdh23 mice (Cdh23tm2.1Kjn/J, JAX: 018399; 4 males and 2
108 females, age 3-8 months). This mouse line has a targeted point reversion in the Cdh23 gene that
109 protects against the age-related hearing loss common to C57BL/6 strains (Johnson et al., 2017).
110 Animals were housed on a reversed 12-hour light–dark cycle with water and food available ad libitum.
111 All procedures were approved by the University of Pennsylvania IACUC and the AALAC Guide on
112 Animal Research. We made every attempt to minimize the number of animals used and to reduce
113 pain or discomfort.

114

115 *Virus injection*

116 Mice were continuously anesthetized with isoflurane and mounted in a stereotaxic frame. Buprenex
117 (0.1 mg/kg), Meloxicam (5 mg/kg) and Bupivicane (2 mg/kg) were injected subcutaneously for
118 preoperative analgesia. We performed small craniotomies bilaterally over AC (−2.6 mm caudal to
119 Bregma, ±4.3 mm lateral, +1 mm ventral) and IC (−4.96 mm caudal to Bregma, ±0.5 mm lateral, +0.5
120 mm ventral and −4.96 mm caudal to Bregma, ±1.25 mm lateral, +1.0 mm ventral). A glass syringe
121 (30-50 μm diameter) connected to a pump (Pump 11 Elite, Harvard Apparatus) was used to inject
122 modified viral vectors (AAV9-CAG-FLEX-ArchT-tdTomato or AAV9-CAG-FLEX-tdTomato;
123 UNC Vector Core) into AC and a retroAAV construct (retro AAV-hSyn-Cre-GFP) into IC (Figure
124 1A, 2A, S1A). We implanted fiber-optic cannulas (Thorlabs, Ø200 μm Core, 0.22 NA) bilaterally
125 over AC injection sites (0.4 mm ventral to brain surface) and secured them in place with dental cement
126 (C and B Metabond) and acrylic (Lang Dental). IC injection sites were covered with a removable
127 silicone plug (Kwik-Sil). A custom-built headplate was secured to the skull at the midline and a
128 ground-pin was lowered into a small craniotomy over Bregma. We injected an antibiotic (5 mg/kg
129 Baytril) subcutaneously for four days postoperatively. Virus injection sites were confirmed
130 postmortem for all animals included in the study.

131

132 *Extracellular recordings*

133 We performed recordings a minimum of 21 days after virus injection surgeries to allow adequate
134 travel time for the viral constructs (Figure 1A). Recordings were carried out inside a double-walled
135 acoustic isolation booth (Industrial Acoustics) or a custom-built table-mounted acoustic isolation
136 booth. For IC recordings, mice were briefly anesthetized to remove the silicone plug over IC virus

injection sites. Following recovery from anesthesia, the headplate was clamped within a custom base to provide head-fixation. We lowered a 32-channel silicon probe (Neuronexus) vertically into IC during presentation of broadband noise clicks and monitored sound responses online to confirm localization within IC (Figure 1A). In each animal, two recordings were performed per IC (four total recording sessions bilaterally). Following completion of all IC recording sessions, we recorded the activity of neurons in AC using the same procedure (Figure 2B). We performed a square craniotomy (2 mm x 2 mm) over AC and oriented the probe vertically to the cortical surface (35-degree angle of the stereotaxic arm). Electrophysiological data were filtered between 600 and 6000 Hz to isolate spike responses and then digitized at 32 kHz and stored for offline analysis (Neuralynx). For a subset of recordings, the experimental procedures were repeated after the animal, while still head-fixed and with the probe left in place, had been anesthetized with isoflurane (Figure 4A). We performed spike sorting using Kilosort2 software (https://github.com/MouseLand/Kilosort). Both single and multi-units were included for all analyses (experimental: 50 single units, 354 multi-units; control: 17 single units; 111 multi-units; anesthetized: 10 single units, 129 multi-units; AC: 95 single units, 300 multi-units; putative cortico-collicular: 9 single units; 11 multi-units).

Laser photo-suppression

We photo-suppressed cortico-collicular neurons using a 532 nm DPSS laser (GL532T3-300, Slocs lasers, 3 mW power at cannula tip or OptoEngine, MGL-III-532, 15 mW power at cannula tip) connected via optical fibers to the implanted cannulas (Figure 1A, 2C, 2D). Data collected using either laser was pooled together, as no significant differences were observed in the strength of photo-suppression in AC during silence ($p=0.054$, Wilcoxon rank sum test) or the presentation of pure tone stimuli ($p=0.072$, Wilcoxon rank sum test) between the two lasers. Square laser pulses were timed to coincide with tone onset and lasted for 100 ms. Evidence of photo-suppression in putative cortico-collicular neurons (infragranular AC neurons with a minimum 30% reduction in both baseline and sound-evoked neuronal activity) was confirmed for all animals included in the study.

Stimuli

We generated an initial frequency response function from a sequence of 50 pure tones, 1-70 kHz, repeated 20 times at 70 dB SPL in pseudo-random order. This response function was generated online to select suitable frequencies for the oddball stimuli, i.e. frequencies that would fall into the average response area for neurons in a given recording. Each tone was 50 ms duration (1 ms cosine squared ramps) with an inter-stimulus interval (ISI) of 200 ms and presentation rate of 4 Hz. A similar

tuning curve stimulus, with 8 amplitude levels (35-70 dB, 5 dB increments) and 5 repetitions, was used to further characterize the tuning properties of each neuron (Figure 3E, 3F).

Oddball tone pairs were chosen to fit within the average response area for neurons from a given recording. Given the prevalence of suppressive regions in the tuning curves, and the fact that this often led to differences in the response profile of the neuron to each frequency in the oddball tone pair, the responses to each frequency were analyzed separately (Figure 3F). Oddball stimuli consisted of a frozen sequence of two pure tones (with the same tone parameters as those used in the initial frequency response functions) with a 90:10 standard-to-deviant ratio and half-octave frequency separation. The number of standards interleaved between two deviants was counterbalanced and varied between 3 and 17 standards. The stimuli were divided into blocks (with the end of a block defined by the presentation of a deviant), and tone type and laser pairings were alternated on subsequent blocks. For example, on the first block the laser stimulus was paired with the deviant, on the second block it was paired with the last standard, and the corresponding tones in the third block served as controls, with no laser stimulus. The number of preceding standards in the blocks was balanced for all three laser conditions (deviant, last standard, and control). The total number of tones in each sequence was 1250. Two oddball sequences were created, both with the same frozen pattern, but with the frequencies of the standard and the deviant switched.

Cascade sequences consisted of either an ascending or descending set of 10 evenly spaced (half-octave separation) pure tones (same tone parameters as described above) (Figure 1C). The two tones used in the oddball sequences were always included as adjacent tones in the cascade sequences, though their position within the cascade was varied. To generate the many standards control sequence, we shuffled the cascade sequences using an algorithm that does not allow for repetition of tones of the same frequency on subsequent presentations.

Analysis

To distinguish between shell and central IC recording locations, we plotted the best frequency for each neuron from a given recording against its depth and fit the data with a robust linear regression model (Figure 3B). Additionally, we computed the mean sparsity for all neurons from a given recording site to quantify the sharpness of tuning. The R^2 metric from the linear fit and the mean sparsity from each recording were used to perform k-means clustering with two groups. Each recording was assigned to a location (either central or shell) according to the k-means output, with central sites typically having high sparsity and high R^2 values and shell sites having low sparsity and low R^2 metrics (Figure 3C).

The threshold for significant sound responsiveness was an absolute value greater than the mean plus three standard deviations of the baseline activity in the 50 milliseconds prior to tone onset. For neurons showing significant sound responses, additional response profiles were assigned for each tone in the oddball pair based on the number, timing, duration, and direction of peaks in the peristimulus time histogram. Neurons with only suppressive or offset responses were removed from the data set.

Significant adaptation or facilitation for each neuron was assessed with a Wilcoxon rank sum test between the trial-by-trial firing rates to the standard and deviant. The index of neuronal mismatch (iMM), equivalent to the SSA index, was further deconstructed into an index of prediction error (iPE) and an index of repetition suppression (iRS) such that iMM = iPE and iRS. The firing rates to the standard, cascade, and deviant conditions were normalized by dividing by the Euclidean norm, N = $\sqrt{{FR_{Dev}}^2 + {FR_{Casc}}^2 + {FR_{Stan}}^2}$. The iPE was calculated as the difference in normalized firing rate to the deviant and cascade conditions (iPE = $\frac{FR_{Dev}}{N}$ - $\frac{FR_{Casc}}{N}$), while the iRS was calculated as the difference in normalized firing rate to the cascade and standard conditions (iRS = $\frac{FR_{Casc}}{N}$ - $\frac{FR_{Stan}}{N}$).

Statistical analysis

Shapiro-Wilk tests were used to assess normality. For normally distributed data, Student's t-tests were performed. When the assumption of normality was violated, Wilcoxon rank sum tests were used for nonpaired data and Wilcoxon signed rank tests were used for paired data.

RESULTS

Experimental design

We used a Cre/FLEX viral injection strategy to selectively express the inhibitory opsin, ArchT, in cortico-collicular neurons of four mice by injecting a retroAAV-Cre-GFP construct into IC and an AAV9-FLEX-ArchT-tdTomato construct into AC (Figure 1A, left). The retroAAV-Cre-GFP construct is transported in a retrograde fashion and expressed in neurons that project to IC (Blackwell et al., 2020). The genes encoded in the AAV9-FLEX-ArchT-tdTomato construct can only be expressed in neurons containing the Cre construct, thereby limiting ArchT expression to neurons in AC that project to IC. In the presence of green light, ArchT, a light-driven outward proton pump, mediates rapid, reversible suppression of the neurons in which it is expressed (Han et al., 2011).

We implanted cannulas over AC in mice injected with the Cre/FLEX constructs and a 532 nm laser was used to provide green light illumination to the region, allowing for suppression of cortico-collicular neurons (Figure 1A, right). The mice were head-fixed and a 32-channel probe was lowered into IC to perform awake extracellular recordings (Figure 1A). Auditory stimuli consisted of oddball sequences of two repeated pure tones, presented at a 90:10 standard-to-deviant ratio and half-octave frequency separation (Figure 1B). On a subset of trials, presentations of either the deviant or the last standard prior to the deviant were coupled with activation of the green laser (Figure 1B, right).

Neurons that displayed a significantly higher response to the deviant than the standard were designated as “adapting” neurons, while those that exhibited a significantly higher response to the standard than the deviant were categorized as “facilitating” neurons (Figure 1D). The difference in firing rate to the standard and deviant was quantified with an index of neuronal mismatch (iMM), which is equivalent to the SSA index used in previous studies (Parras et al., 2017).

A cascade stimulus consisting of 10 evenly spaced tones, including the tone pair from the oddball sequence, was presented to further decompose the neuronal mismatch between the responses to the standard and deviant (Figure 1C, 1D). This stimulus is unique in that each tone occurs with the same likelihood as the deviant tone in the oddball stimulus (10%), but it contains no true statistical deviants: each tone has the same likelihood of presentation, and the tone sequence overall follows a regular and predictable pattern (Parras et al., 2017). Therefore, the response to a given tone when it is embedded in the cascade can be compared to the response when it is a deviant in order to isolate prediction error effects (Figure 1C; 1D, top). A neuron exhibits prediction error if it fires more strongly to a tone when it is a deviant than when it is presented in the cascade sequence (Figure 1D, top). Conversely, if a neuron responds more strongly to a tone presented in the cascade sequence than when it is a deviant, the neuron encodes error suppression (Figure 1D, bottom). This phenomenon is

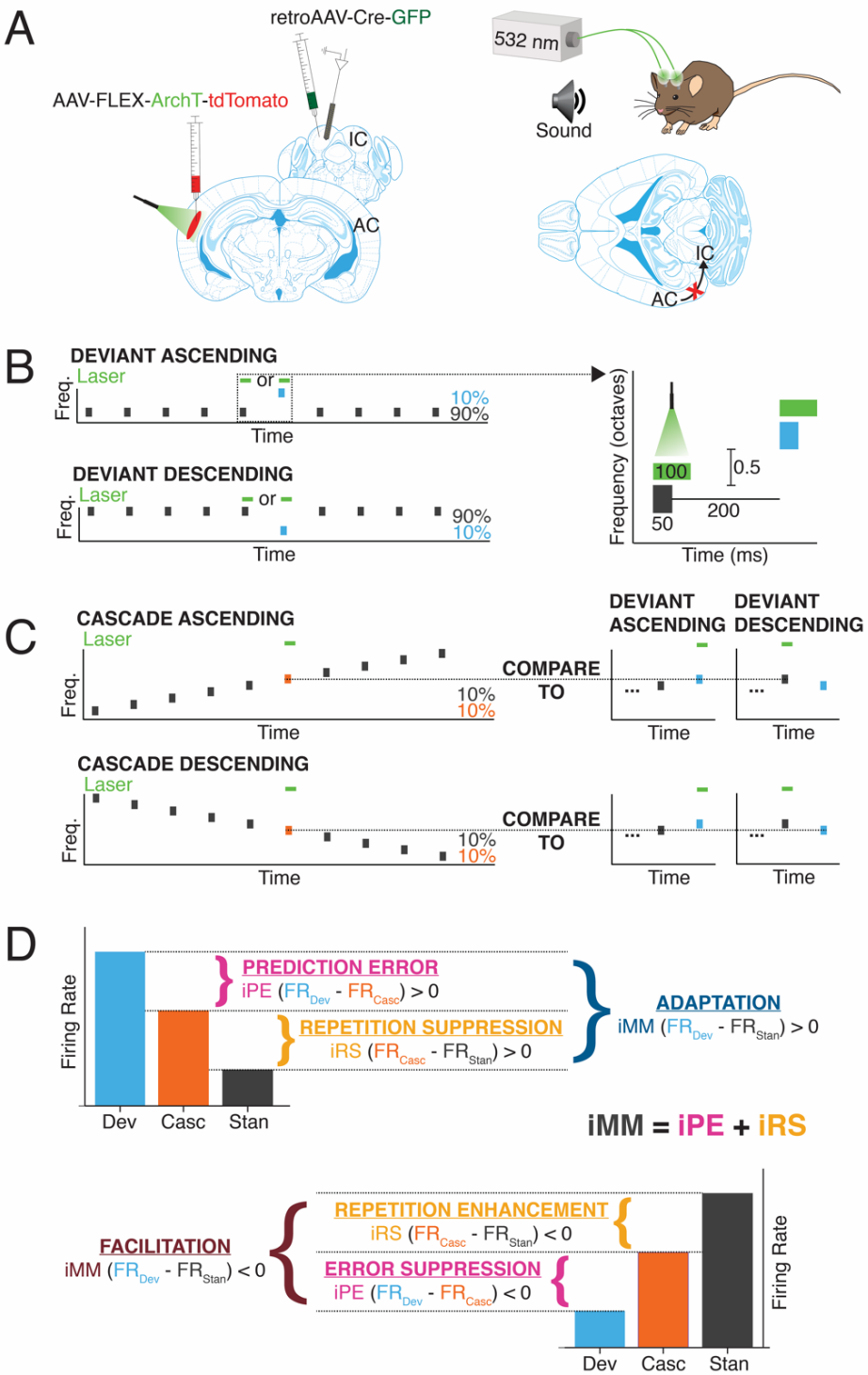

Figure 1: Experimental design. A) Cre/FLEX dual injections for selective ArchT expression in cortico-collicular neurons. Recordings were performed in IC while photo-suppression was mediated by a 532 nm laser connected to cannulas implanted over AC. B) Oddball stimuli consisted of pairs of pure tones separated by 0.5 octave with a 90:10 standard-to-deviant ratio. Two sequences were constructed such that each frequency is represented as both the standard and the deviant. C) Cascade sequences consisted of 10 evenly spaced tones separated by 0.5 octaves, with both frequencies from the oddball sequence included in the sequence. Responses to tones in the cascade context were compared to responses in the standard and deviant context to analyze repetition and prediction effects, respectively. D) A positive iMM (top diagram) indicates a stronger response to the deviant than the standard (adaptation), while a negative iMM (bottom diagram) indicates a stronger response to the standard than to the deviant (facilitation). The iMM can be further decomposed into an iPE and an iRS. Positive iPE values represent prediction error and negative values convey error suppression. Positive iRS indices indicate repetition suppression, while repetition enhancement is represented by negative values.

quantified using an index of prediction error (iPE), with positive indices indicating prediction error and negative indices representing error suppression (Figure 1D).

The cascade sequence is also free from repetition effects, since adjacent tone presentations never include a tone of the same frequency (Figure 1C). Therefore, the response to a given tone embedded in the cascade sequence can be compared to the response generated when that tone is a standard. The difference in response indicates either repetition suppression (stronger response to the tone in the cascade) (Figure 1D, top) or repetition enhancement (stronger response to the tone as a standard) (Figure 1D, bottom). These contrasting processes are quantified by the index of repetition suppression (iRS), with a positive index indicating repetition suppression and a negative index representing repetition enhancement (Figure 1D).

Cre/FLEX viral injection strategy enables selective suppression of cortico-collicular neurons

Examination of fixed tissue from injected mice revealed that expression of the retroAAV-Cre-GFP construct was restricted to IC (Figure 2A, top left). Somatic expression of tdTomato (indicating the presence of ArchT) was restricted to layer 5 and deep layer 6 of AC, which contain cortico-collicular cell bodies (Figure 2A, right) (Bajo et al., 2007; Schofield, 2009; Yudintsev et al., 2019). Axons and terminals labeled with tdTomato were distributed in IC in a manner matching the known projection pattern of this pathway, with dense, "patchy" labeling in shell regions of IC (Figure 2A, bottom left) (Herbert et al., 1991; Lesicko et al., 2016; Saldaña et al., 1996; Torii et al., 2013). These data confirm that our viral injection strategy leads to selective transfection of cortico-collicular neurons.

Extracellular recordings in AC of injected mice revealed a reduction in firing rate during the duration of the laser stimulus in a number of neurons (Figure 2B, 2C). In these putative cortico-collicular neurons, laser-induced suppression led to a mean ~60% reduction in firing rate at baseline (Figure 2C, left; 2D, top; Table 1; p=1.9e-06, Wilcoxon signed rank test) and an average ~45% reduction in firing during presentation of pure tone stimuli (Figure 2C, right; 2D, bottom; Table 1; p=1.9e-06, Wilcoxon signed rank test). These results indicate that our optogenetic parameters succeed in significantly suppressing cortico-collicular neurons.

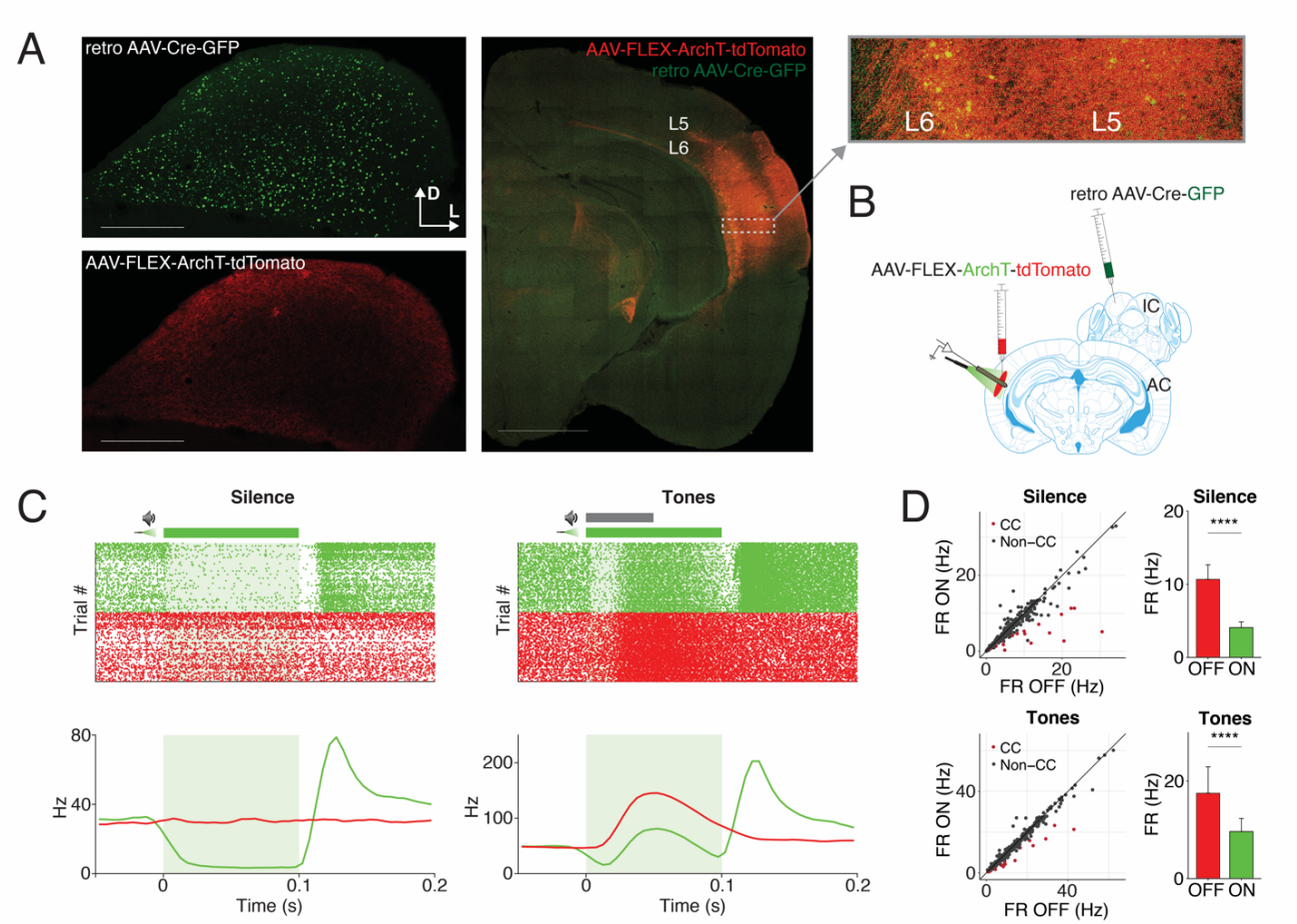

Figure 2: Cre/FLEX viral injection strategy enables selective suppression of cortico-collicular neurons. A) Expression of the retroAAV-Cre-GFP construct at the injection site is restricted to IC (top left). tdTomato labeled axons are found in a pattern matching the known topographical distribution of cortico-collicular neurons in IC (left bottom). Somatic AAV9-FLEX-ArchT-tdTomato expression is present in layer 5 and 6 of AC (right, inset). B) Experimental design for recording from AC to confirm presence of photo-suppressed neurons. C) Example of a photo-suppressed neuron (i.e. putative cortico-collicular neuron) exhibiting a strong reduction in firing during silence and during the presentation of pure tones. D) Population data demonstrating reduced firing rates during silence and in response to pure tone stimuli in putative cortico-collicular neurons. Dots represent individual neurons. Bar plots represent means over the population n = 20 CC neurons. Error bars are standard error of the mean.

Sound responses in the awake IC are complex and heterogenous

Shell and central regions of IC differ in their tuning, degree of adaptation, and amount of input from AC, and may also play distinct roles in predictive processing (Aitkin et al., 1975; Bajo et al., 2007; Blackwell et al., 2020; Duque et al., 2012; Herbert et al., 1991; Stebbings et al., 2014; Syka et al., 2000). We subdivided the recording sites by exploiting known differences in the sharpness of tuning and direction of frequency gradients between shell and central regions (Figure 3A) (Aitkin et al., 1975; Chen et al., 2012; Malmierca et al., 2008; Stiebler & Ehret, 1985; Syka et al., 2000). We performed clustering analysis using the mean sparsity and variation in best frequency with depth from each recording site to determine whether it was from the central nucleus or shell regions of IC (Figure 3B, 3C).

IC neurons exhibited multiple types of responses to pure tone stimuli (Figure 3D). In addition to excitatory responses (e.g. onset and sustained responses), suppressed responses were common, as has previously been characterized in IC of awake animals (Figure 3D, top right, bottom middle) (Duque & Malmierca, 2015). Consistent with previous findings, tuning curves from central regions were sharp and narrow, whereas neurons in shell regions exhibited broad frequency tuning (Figure 3E, left vs. right) (Aitkin et al., 1975; Syka et al., 2000). Suppressive side-bands were common in tuning curves from both regions, and some suppressive tuning curves were observed (Figure 3F). These data confirm that our experimental parameters elicit sound responses and tuning properties characteristic of central and shell regions of the awake IC (Aitkin et al., 1975; Duque & Malmierca, 2015; Syka et al., 2000).

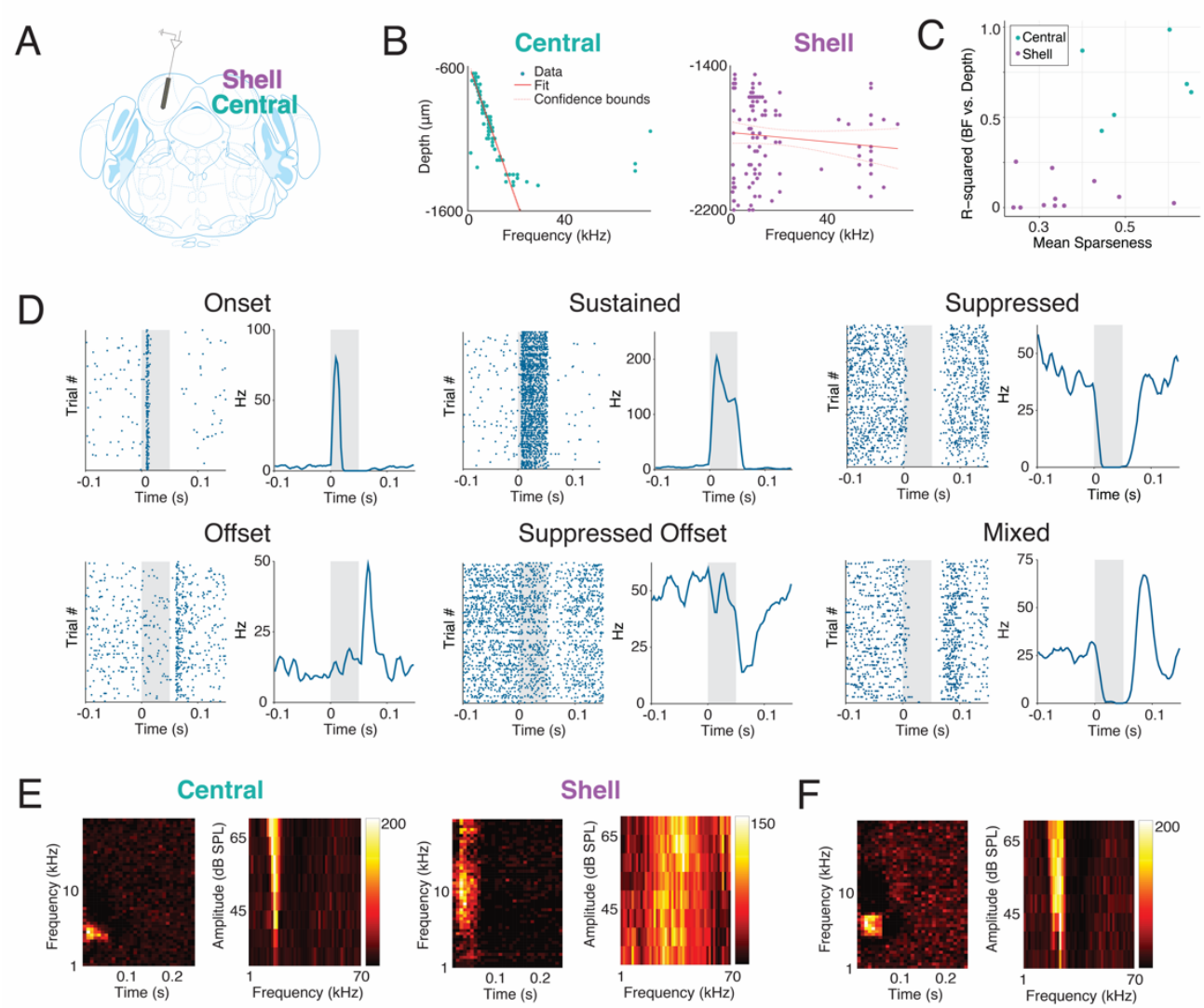

Figure 3: Sound responses in the awake IC are complex and heterogenous. A) Experimental design for awake IC recordings in the central and shell regions of IC. B) Linear fits for best frequency vs. depth in central (left) and shell (right) IC. C) Sparseness vs. R^2 value for linear fit. K-means clustering was performed using these parameters to classify recording sites as either in the shell or central nucleus of IC. D) Example raster plots and peristimulus time histograms showing different firing types in the awake IC. E) Example tuning curves in central (left) and shell (right) IC. F) Example of a tuning curve with suppressive side-bands.

IC neurons encode different aspects of prediction and repetition in awake and anesthetized states

Much of the research regarding deviance detection in IC to date has been performed in anesthetized animals, with few studies recording from awake subjects (Duque & Malmierca, 2015; Parras et al., 2017). Given that neuronal responses to sound depend on the state of anesthesia of the subject, it is possible that metrics of deviance detection in the awake IC differ from what has previously been characterized in anesthetized animals (Fontanini & Katz, 2008; Gaese & Ostwald, 2001; Schumacher et al., 2011). To investigate this possibility, in a subset of animals we first performed awake recordings and then repeated our experimental procedures, leaving the animal head-fixed and the probe in place, after anesthetizing the mouse with isoflurane (Figure 4A). This protocol allowed us to compare how metrics of deviance detection differ between the awake and anesthetized preparations in the same population of neurons.

In the central IC, the distribution of iMM values in the anesthetized condition was positively skewed with a mean iMM of 0.25, indicative of prevalent adaptation (Figure 4B). The iMM values under anesthesia were significantly higher than those obtained while the animal was awake (Figure 4B, Table 1; p=0.039, Student's t-Test). To better understand whether prediction or repetition effects underlie iMM in each condition, the iMM for both distributions was further decomposed into an iPE and iRS. In the anesthetized condition, the mean iPE value of 0.018 indicated modest prediction error, while a negative iPE value of -0.15 in the awake condition indicated error suppression (Figure 4C). Under both anesthetized and awake conditions, prominent repetition suppression was observed in the central IC (Figure 4D).

Similar to the central IC, the mean iMM was significantly more positive in shell regions during anesthesia (Figure 4E, Table 1; p=1.5e-08, Wilcoxon signed rank test). A greater proportion of neurons in the awake condition had a negative iMM compared with the anesthetized distribution, indicating that facilitation (a greater response to the standard than the deviant context) is more common in the awake than the anesthetized condition (Figure 4E). The iPE values in shell IC suggest that prediction error is significantly higher in the awake compared to the anesthetized condition (Figure 4F, Table 1; p=2.2e-05, Wilcoxon signed rank test). Although the distribution for the iRS under anesthesia was positively skewed with a mean of 0.22, indicating prevalent repetition suppression, the awake distribution exhibited a significant leftward shift by comparison (Figure 4G). Interestingly, the mean iRS for the awake condition was negative (mean=-0.13), indicating that repetition *enhancement*, rather than suppression, is present in the awake shell IC (Figure 4G, Table 1; p=2.1e-14, Wilcoxon signed rank test). These results point to differences between deviance metrics

in the awake and anesthetized states, with previously undescribed metrics such as repetition enhancement and error suppression present only in awake animals.

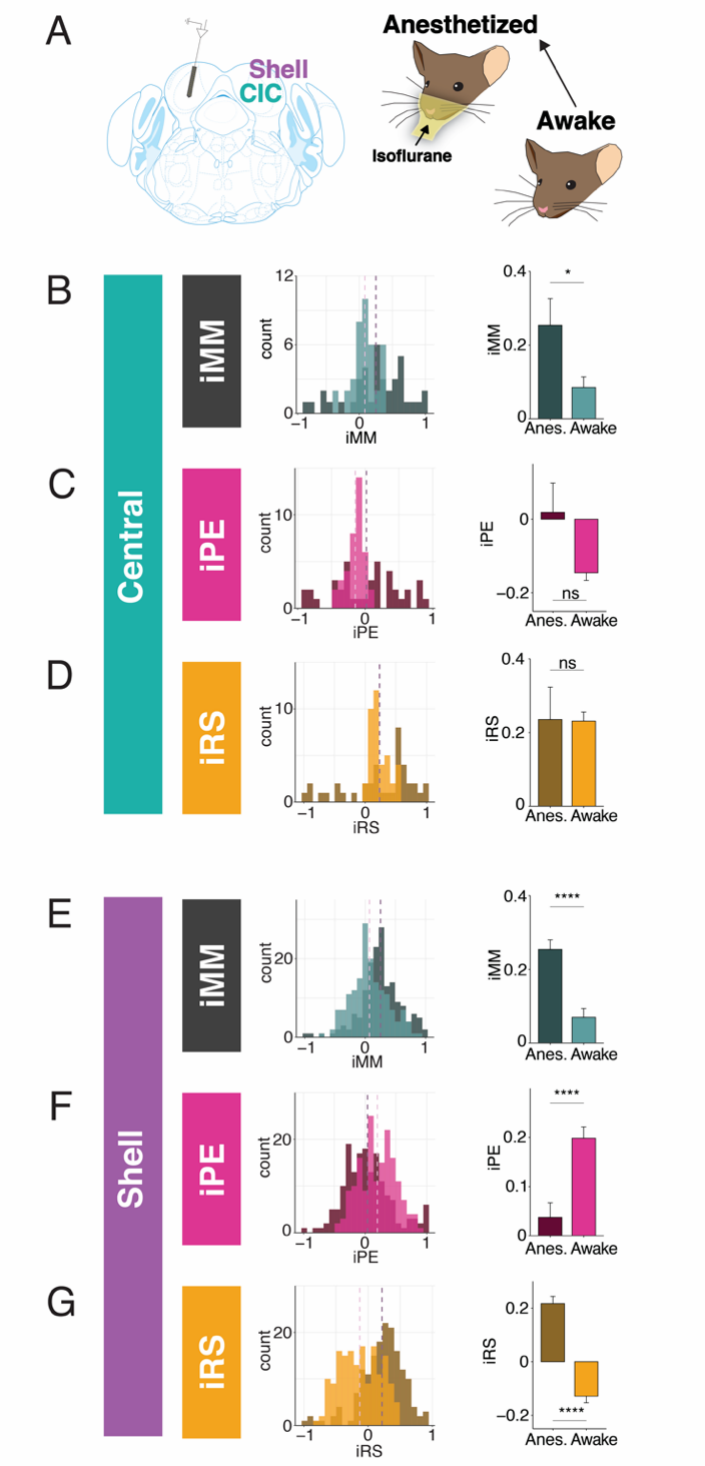

Figure 4: IC neurons encode different aspects of prediction and repetition in awake and anesthetized states. A) Experimental design for recording in the awake and isoflurane anesthetized IC in the same population of neurons. B) Distribution of iMM in the awake vs. anesthetized central IC. Bar plots represent means over the population of n = 39 neurons. Error bars are standard error of the mean. C) iPE distribution in the awake vs. anesthetized central IC. D) iRS distribution in the awake vs. anesthetized central IC. E) Distribution of iMM in the awake vs. anesthetized shell IC. Bar plots represent means over the population of n = 165 neurons. Error bars are standard error of the mean. F) iPE distribution in the awake vs. anesthetized shell IC. G) iRS distribution in the awake vs. anesthetized shell IC.

374 *Adapting and facilitating neurons are differentially affected by cortico-collicular suppression*

375 We next performed recordings in IC of awake mice to determine how neuronal mismatch and
376 its component repetition and prediction metrics were affected by cortico-collicular suppression
377 (Figure 5A). To suppress cortico-collicular feedback, we shined light over AC in subjects which
378 expressed a suppressive opsin in cortico-collicular neurons. We segregated the population of recorded
379 neurons according to those that exhibited a significantly stronger response to the deviant than the
380 standard (adapting neurons; Figure 5B, blue; 5C), those that exhibited a significantly stronger
381 response to the standard than the deviant (facilitating neurons; Figure 5B, red; 5F), and those that
382 responded equally to both stimulus contexts (non-adapting neurons; Figure 5B, green) for recordings
383 in both central and shell regions of IC (Figure 5B, left vs. right).

384 The iMM for adapting neurons in the central nucleus significantly decreased with laser photo-
385 suppression of cortico-collicular neurons (Figure 5D, top; Table 1; p=0.00034, Wilcoxon signed rank
386 test). The iMM at baseline for adapting neurons predominantly represents repetition suppression
387 (Figure 5D, bottom) and a small amount of prediction error (Figure 5D, middle). Prediction error was
388 abolished during laser photo-suppression (Figure 5D, middle; Table 1; p=0.048, Wilcoxon signed
389 rank test), while repetition suppression remained unaffected (Figure 5D, bottom). Adapting neurons
390 in shell regions of IC exhibited a similar pattern to those in the central nucleus. At baseline, these
391 neurons encoded both prediction error and repetition suppression (Figure 5E, middle and bottom). A
392 significant decrease in iMM during laser suppression (Figure 5E, top; Table 1; p=0.0023, Wilcoxon
393 signed rank test) was driven by a decrease in prediction error (Figure 5E, middle; Table 1; p=0.034,
394 Wilcoxon signed rank test), whereas repetition suppression remained unaffected (Figure 5E, bottom).
395 Combined, these results suggest that removing cortical feedback reduced prediction error but not
396 repetition suppression in adapting neurons.

397 Prior studies of deviance detection in IC have focused exclusively on adapting neurons.
398 However, given the relative prevalence of facilitating neurons discovered in the awake versus
399 anesthetized IC (Figure 4), we further investigated this population of neurons to determine whether
400 facilitation reflects prediction or repetition effects. In the central nucleus, cortico-collicular
401 suppression led to a significant decrease in facilitation in facilitating neurons (Figure 5G, top; Table
402

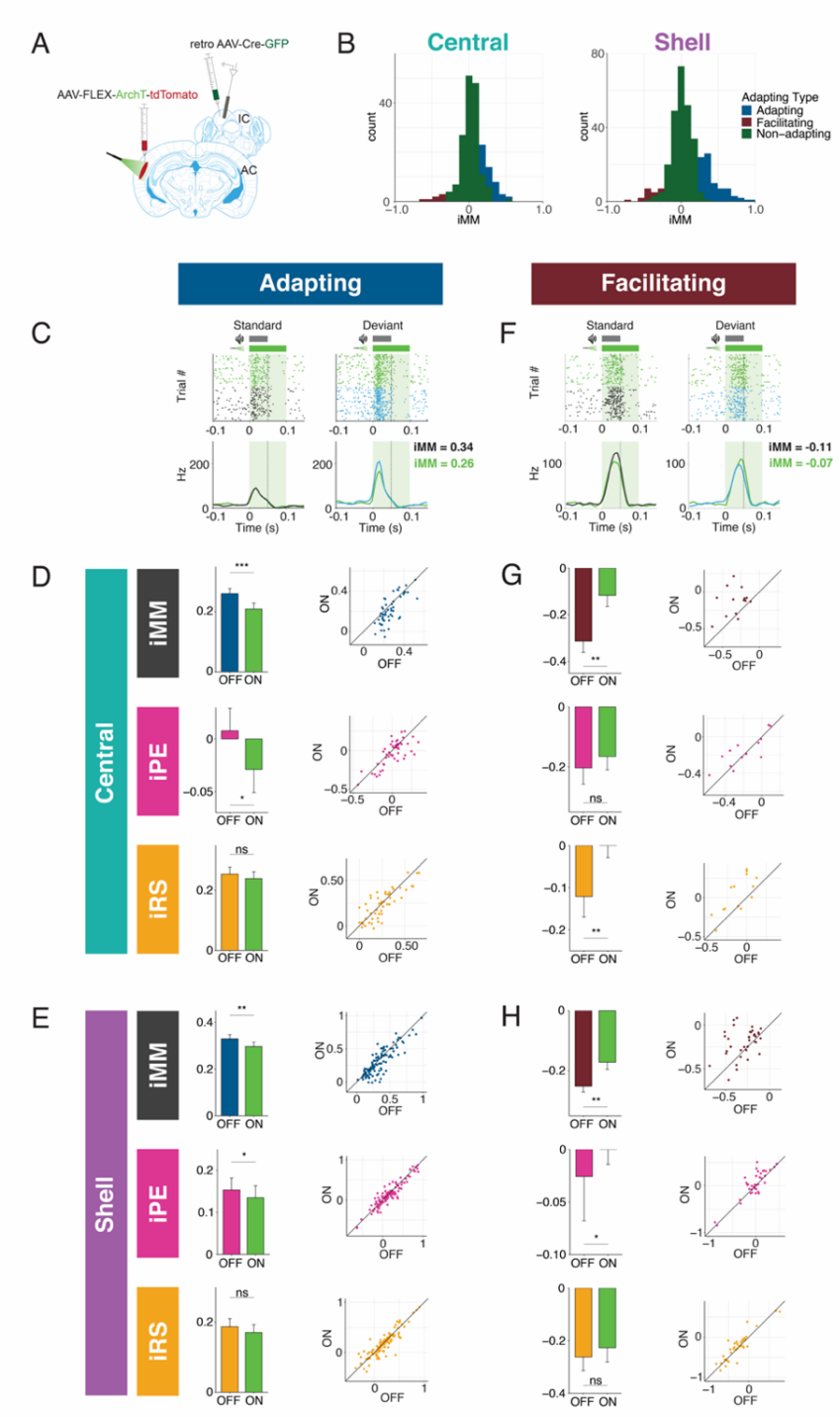

Figure 5: Adapting and facilitating IC neurons are differentially affected by cortico-collicular suppression. A) Experimental design for recording in awake IC during laser photo-suppression of the cortico-collicular pathway. B) Categorization of neurons according to whether they displayed significant adaptation, facilitation, or neither (non-adapting). C) Example raster plot and peristimulus time histogram for an adapting neuron in IC. Green = during laser photo-suppression. D) iMM (top), iPE (middle), and iRS (bottom) for adapting neurons in the central nucleus. Dots represent individual neurons. Bar plots represent means over the population of n = 52 neurons. Error bars are standard error of the mean. E) iMM (top), iPE (middle), and iRS (bottom) for adapting neurons in shell regions of IC. Dots represent individual neurons. Bar plots represent means over the population of n = 113 neurons. Error bars are standard error of the mean. F) Example raster plot and peristimulus time histogram for a facilitating neuron in IC. Green = during laser photo-suppression. G) iMM (top), iPE (middle), and iRS (bottom) for facilitating neurons in the central nucleus. Dots represent individual neurons. Bar plots represent means over the population of n = 14 neurons. Error bars are standard error of the mean. H) iMM (top), iPE (middle), and iRS (bottom) for facilitating neurons in shell regions of IC. Dots represent individual neurons. Bar plots represent means over the population of n = 38 neurons. Error bars are standard error of the mean.

1; p=0.0036, Student's t-Test). At baseline, the iMM for facilitating neurons represents a combination of error suppression and repetition enhancement (Figure 5G, middle and bottom). During photo-suppression, error suppression remained unaffected (Figure 5G, middle), while repetition enhancement was nearly abolished (Figure 5G, bottom; Table 1; p=0.0026, Student's t-Test). Facilitating neurons in the shell IC were also significantly affected by cortico-collicular suppression (Figure 5H, top; Table 1; p=0.0016, Wilcoxon signed rank test). In this case, however, the change in iMM was driven by the near abolishment of error suppression (Figure 5H, middle; Table 1; p=0.037, Wilcoxon signed rank test), while repetition enhancement was unaffected (Figure 5H, bottom).

These data suggest that adaptation and facilitation in the awake IC are composed of distinct underlying processes: adapting populations in both central and shell regions of IC exhibit prediction error and repetition suppression, while facilitating populations are characterized by error suppression and repetition enhancement. In adapting neurons in both central and shell regions, cortico-collicular photo-suppression significantly decreases prediction error. Facilitating neurons in the central IC display decreased repetition enhancement with cortico-collicular photo-suppression, while those in shell regions exhibit decreased error suppression.

To ensure that the laser-induced changes described above were opsin-mediated, we performed control experiments in two mice with identical manipulations to the experimental group, but in the absence of ArchT (Figure S1A). At baseline, the control group exhibited a similar distribution of iMM values to the experimental group in both the central and shell regions of IC (Figure S1B, Table 2). We found no significant differences between baseline and laser trials for either adapting (Figure S1C, S1D, Table 2) or facilitating (Figure S1E, S1F) neurons in either region. This experiment confirmed that the observed effects of cortico-collicular suppression were indeed due to opsin-mediated suppression of the cortico-collicular projection neurons.

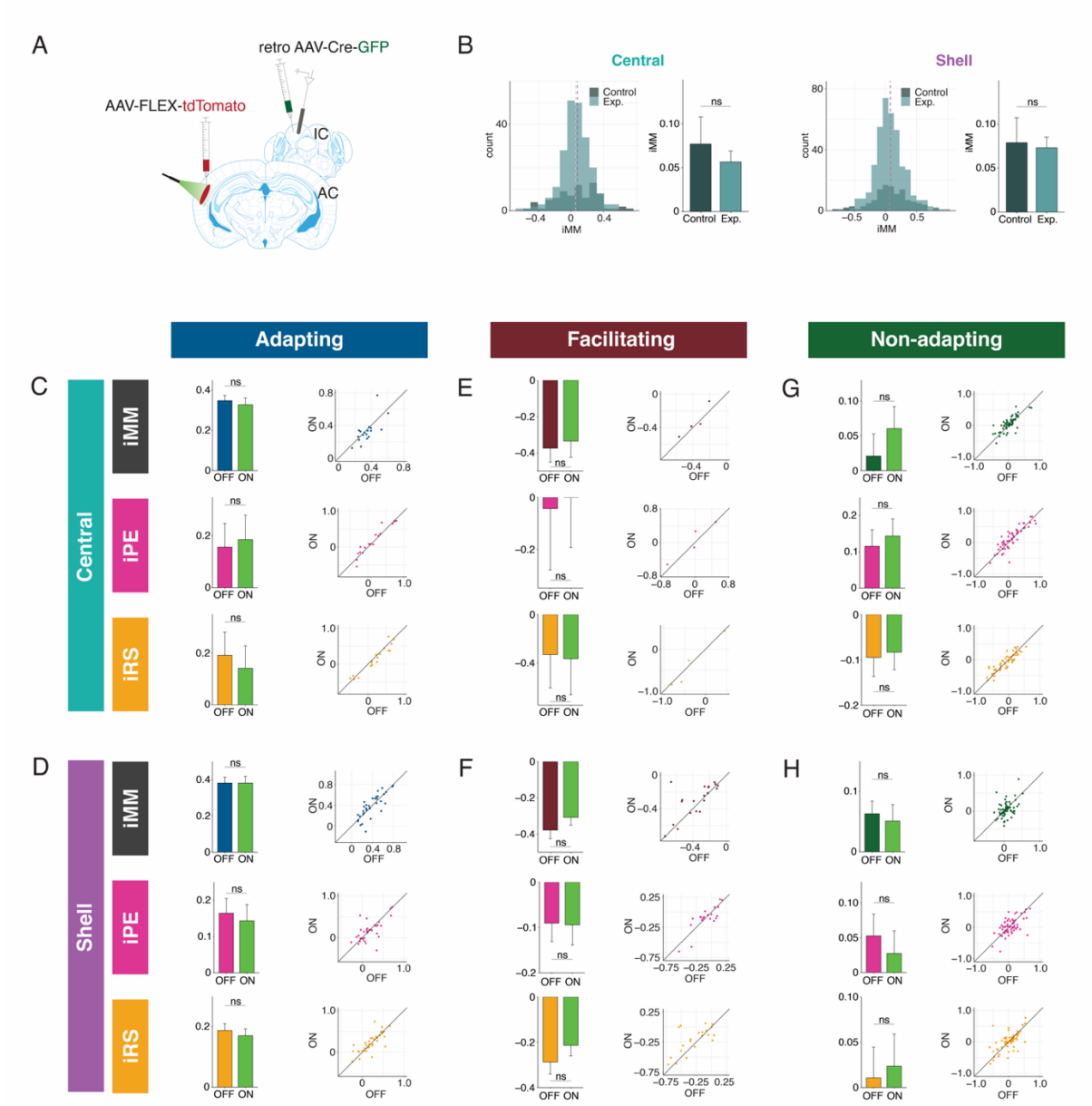

Supplementary Figure 1: Control data. A) Experimental design for control experiments. All procedures were performed identically to the experimental group, except with the omission of ArchT from the viral construct injected in AC. B) Comparison of iMM distribution for control (navy) and experimental (light blue) groups in central (left) and shell (right) IC. C) iMM (top), iPE (middle), and iRS (bottom) for control adapting neurons in the central nucleus. Dots represent individual neurons. Bar plots represent means over the population of n = 18 neurons. Error bars are standard error of the mean. D) iMM (top), iPE (middle), and iRS (bottom) for control adapting neurons in shell regions of IC. Dots represent individual neurons. Bar plots represent means over the population of n = 35 neurons. Error bars are standard error of the mean. E) iMM (top), iPE (middle), and iRS (bottom) for control facilitating neurons in the central nucleus. Dots represent individual neurons. Bar plots represent means over the population of n = 4 neurons. Error bars are standard error of the mean. F) iMM (top), iPE (middle), and iRS (bottom) for control facilitating neurons in shell regions of IC. Dots represent individual neurons. Bar plots represent means over the population of n = 21 neurons. Error bars are standard error of the mean. G) iMM (top), iPE (middle), and iRS (bottom) for control non-adapting neurons in the central nucleus. Dots represent individual neurons. Bar plots represent means over the population of n = 55 neurons. Error bars are standard error of the mean. H) iMM (top), iPE (middle), and iRS (bottom) for control non-adapting neurons in shell regions of IC. Dots represent individual neurons. Bar plots represent means over the population of n = 63 neurons. Error bars are standard error of the mean.

Adapting and facilitating neurons respond similarly to the cascade and many standards controls

Though the cascade sequence is free of repetition effects between adjacent tone pairs, it does exhibit global repetition across the entire tone sequence. To assess whether global stimulus regularity affects the response to the cascade context, we used a shuffled version of the cascade sequence, known as the "many standards" sequence, as an additional control stimulus (Figure S2A). The many standards sequence contains the same 10 tones as the cascade but presented in random order (Figure S2A). This reduces the potential for adaptation across adjacent frequency channels and also eliminates the global predictability of the stimulus, both of which could lead to suppression of responses to tones in the cascade context and potentially affect the calculations of iMM, iPE, and iRS. We compared the responses of adapting and facilitating neurons in both central and shell regions of IC to tones in the cascade versus the many standards context (Figure S2A). We found no significant differences in firing rates to the cascade versus the many standards contexts (Figure S2B, S2C, Table 1), suggesting that the global structure of the cascade sequence does not significantly affect how neurons in IC respond to this stimulus.

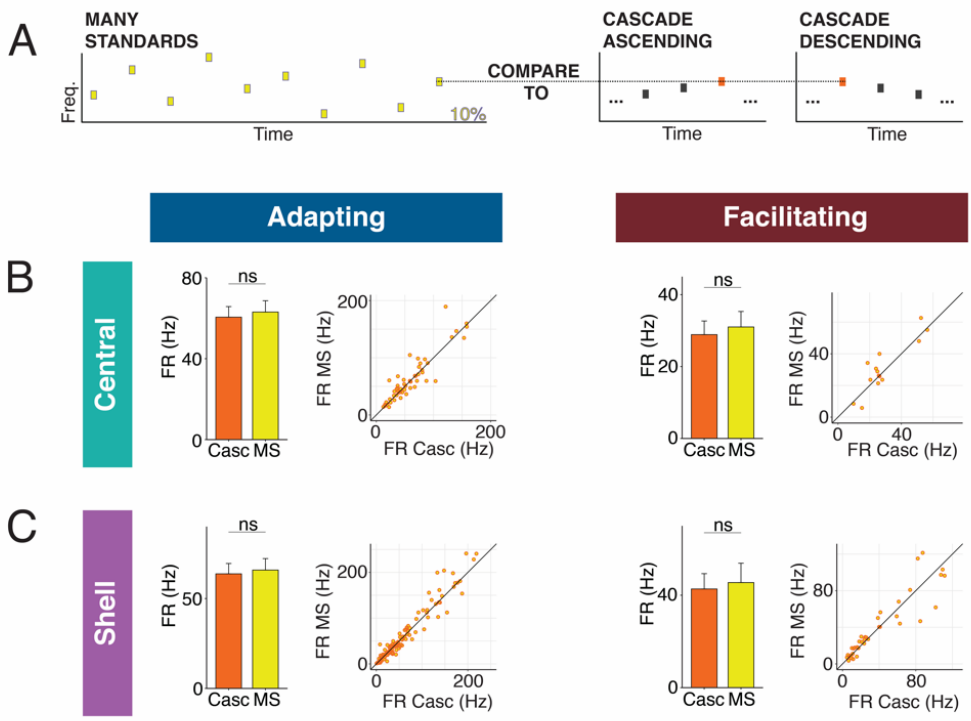

Supplementary Figure 2: Comparison of neuronal responses between the many standards and cascade sequences. A) The many standards sequence consists of the same 10 tones found in the cascade sequence, but the tone order is random. Responses to the cascade and many standards sequences were compared to assess whether cross-frequency adaptation or global stimulus regularity affect responses to the cascade condition. B) Firing rates of adapting neurons (left) and facilitating neurons (right) in the central IC to tones in the cascade and many standards contexts. Dots represent individual neurons. Bar plots represent means over the population of n = 52 adapting and n = 14 facilitating neurons. Error bars are standard error of the mean. C) Firing rates of adapting neurons (left) and facilitating neurons (right) in the shell IC to tones in the cascade and many standards contexts. Dots represent individual neurons. Bar plots represent means over the population of n = 113 adapting and n = 38 facilitating neurons. Error bars are standard error of the mean.

Cortico-collicular suppression also affects non-adapting neurons in awake IC

The vast majority of neurons in both central and shell IC do not exhibit either adaptation or facilitation but respond similarly to tones regardless of the statistical context in which they are presented (Figure 6A). We further characterized these non-adapting neurons (Figure 6B) and tested how they are affected by cortico-collicular suppression. Non-adapting neurons in the central nucleus exhibited a significant increase in iMM during photo-suppression (Figure 6C, top; Table 1; p=2.7e-06, Wilcoxon signed rank test), whereas those in the shell IC were unaffected (Figure 6D, top). The change in iMM for non-adapting neurons in the central nucleus was driven by a significant increase in repetition suppression (Figure 6C, bottom; Table 1; p=0.0011, Wilcoxon signed rank test). In control experiments without ArchT, no significant changes were observed in non-adapting neurons (Figure S1G, S1H, Table 2). These results indicate that AC also regulates metrics of deviance detection in non-adapting neurons, predominantly in the central IC.

Standard and deviant responses are bidirectionally modulated by cortico-collicular suppression

The observed changes in repetition metrics with cortico-collicular suppression could reflect an effect on either the standard or cascade context. Similarly, the shift in prediction metrics observed with photo-suppression could be due to altered responses to either the cascade or deviant contexts. We next determined whether the laser-induced changes in the iMM, the iPE, and the iRS for adapting neurons reflect changes in the firing rates to the standard, deviant, or cascade contexts. We found that adapting neurons in the central nucleus increased responses to the standard (Figure 7A, Table 1; p=0.020, Wilcoxon signed rank test) and decreased responses to the deviant (Figure 7A, Table 1; p=0.0038, Wilcoxon signed rank test) during photo-suppression. These results explain the decrease in iMM for this population during the laser stimulus (Figure 5D, top): the firing rate to the cascade stimulus did not change during cortico-collicular suppression, which means that the decrease in firing rate to the deviant alone underlies the decrease in prediction error seen for this population (Figure 5D, middle). Adapting neurons in the shell exhibited the same pattern of bidirectional changes to the standard (Figure 7B, Table 1; p=0.035, Wilcoxon signed rank test) and deviant (Figure 7B, Table 1; p=0.0057, Wilcoxon signed rank test), similarly accounting for their decrease in iMM and prediction error (Figure 5E), with no change in response to the cascade condition (Figure 7B). These data suggest that suppression of the cortico-collicular pathway induces bidirectional changes in firing rates to the standard and deviant for adapting neurons in both central and shell regions of IC.

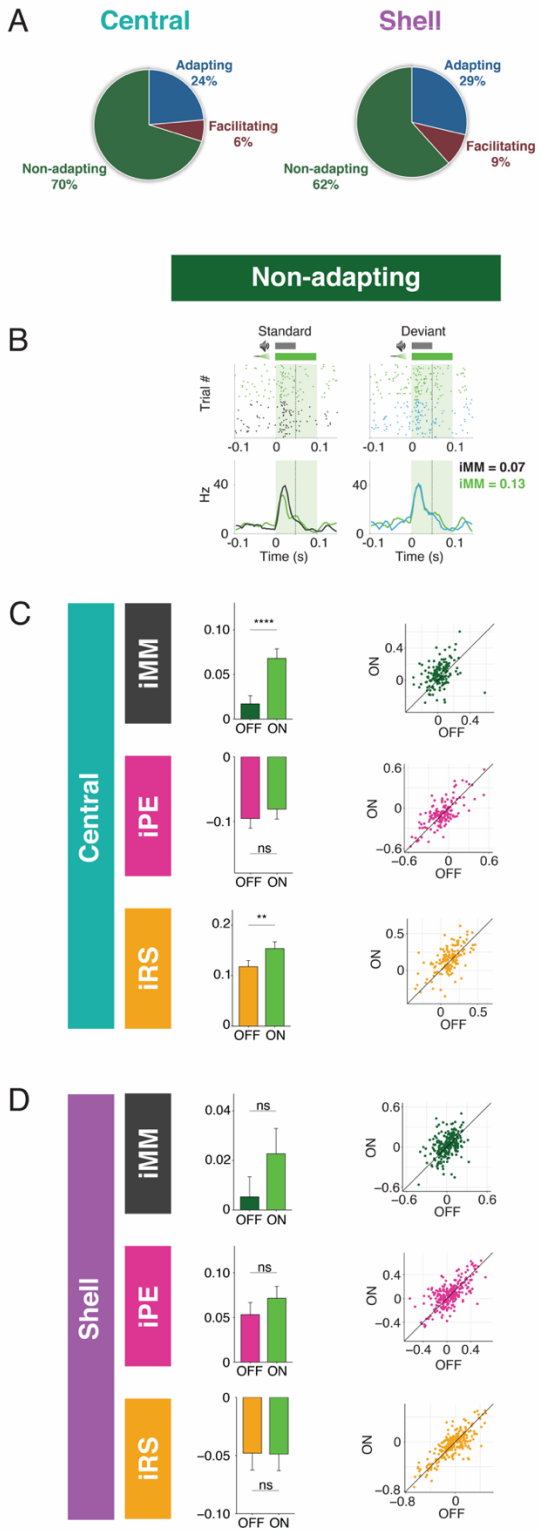

Figure 6: Cortico-collicular suppression also affects non-adapting neurons in awake IC. A) Distribution of adapting types (adapting, facilitating, and non-adapting) for neurons in central (left) and shell (right) regions of IC. B) Example raster plot and peristimulus time histogram for a non-adapting neuron in IC. C) iMM (top), iPE (middle), and iRS (bottom) for non-adapting neurons in central regions of IC. Dots represent individual neurons. Bar plots represent means over the population of n = 155 neurons. Error bars are standard error of the mean. D) iMM (top), iPE (middle), and iRS (bottom) for non-adapting neurons in shell regions of IC. Dots represent individual neurons. Bar plots represent means over the population of n = 243 neurons. Error bars are standard error of the mean.

521 We also investigated how responses to each stimulus context changed with cortico-collicular
522 suppression for facilitating neurons. For central facilitating neurons, only the firing rate to the
523 standard context changed during photo-suppression (Figure 7C, Table 1; p=0.0057, Wilcoxon signed
524 rank test), explaining the observed change in repetition enhancement for this population (Figure 5G).
525 For shell facilitating neurons, a decreased response to the standard (Figure 7D, Table 1; p=0.0055,
526 Wilcoxon signed rank test) and an increased response to the deviant (Figure 7D, Table 1; p=0.0023,
527 Wilcoxon signed rank test) were elicited on laser trials, accounting for changes in the iMM and the
528 abolishment of error suppression (Figure 5H). These changes are directionally opposite to the
529 observed firing rate changes observed for adapting neurons under photo-suppression, with a decrease
530 to the standard context for both central and shell neurons and an increase to the deviant context for
531 shell neurons.
532 For non-adapting neurons, a significant decrease in response to the standard context was
533 observed in both central (Figure 7E, Table 1; p=1.4e-06, Wilcoxon signed rank test) and shell (Figure
534 7F, Table 1; p=0.035, Wilcoxon signed rank test) regions of IC. The decrease was only significant
535 enough to produce an effect on the iMM in central regions (Figure 6C, top), leading to an increase in
536 repetition suppression (Figure 6C, bottom).
537 For adapting and facilitating neurons, these data exhibit that IC responses to the standard and
538 deviant contexts in the absence of cortical input are bidirectionally modulated, such that neurons
539 respond more similarly to both contexts rather than firing differentially to each. For non-adapting
540 neurons, the response to the standard context alone is diminished during cortico-collicular
541 suppression, causing these neurons to become more adapting. These changes suggest that under
542 normal conditions, AC provides information regarding sound context to neurons in IC.
543
544 *Individual neurons have distinct combinations of iPE and iRS*
545 To determine whether sensitivity to repetition and prediction is encoded in distinct neural
546 populations, or whether individual neurons exhibit particular combinations of repetition
547 suppression/enhancement and prediction error/error suppression, we plotted the iPE values against
548 the iRS values for each neuron in the adapting, facilitating, and non-adapting groups. Both the
549 adapting and non-adapting groups in the central IC contained neurons with significant values for both
550 iPE and iRS, most often resulting from a combination of error suppression and repetition suppression
551 (Figure 8A, maroon dots). In the shell IC, a greater variety of response combinations was observed.
552 All three groups contained neurons with both significant error suppression and repetition suppression,

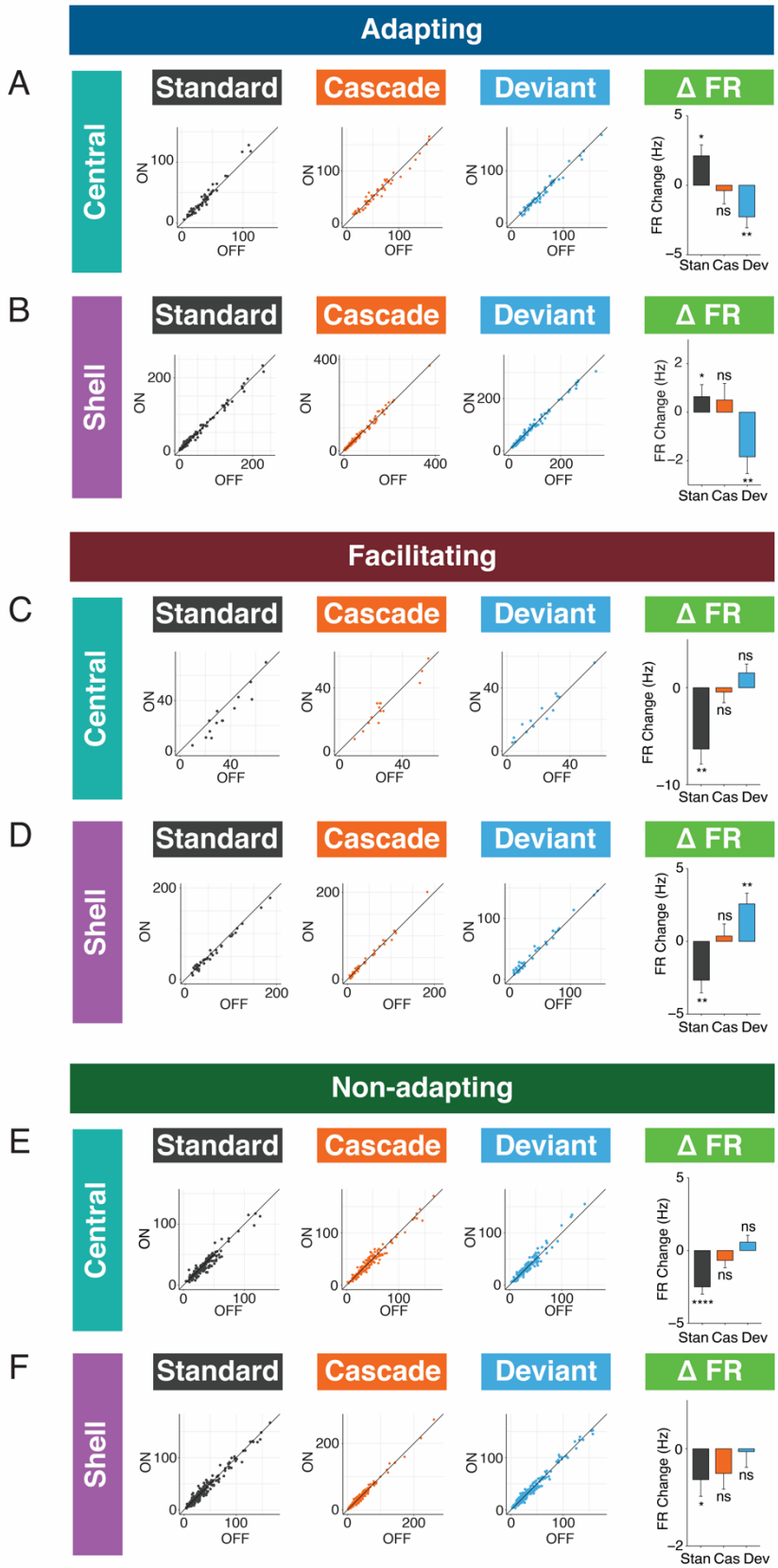
Adapting
A
Central
Standard
Cascade
Deviant
Δ FR
ON
OFF
FR Change (Hz)
Stan Cas Dev
B
Shell
Facilitating
C
D
Non-adapting
E
F

553

Figure 7: Standard and deviant responses are bidirectionally modulated by cortico-collicular suppression. A) Responses to the standard (left), cascade (middle left), and deviant (middle right) for adapting neurons in central regions of IC under baseline and laser conditions. Change in firing rate between the laser and baseline condition for each stimulus (right). Dots represent individual neurons. Bar plots represent means over the population of n = 52 neurons. Error bars are standard error of the mean. B) Responses to the standard (left), cascade (middle left), and deviant (middle right) for adapting neurons in shell regions of IC under baseline and laser conditions. Change in firing rate between the laser and baseline condition for each stimulus (right). Dots represent individual neurons. Bar plots represent means over the population of n = 113 neurons. Error bars are standard error of the mean. C) Responses to the standard (left), cascade (middle left), and deviant (middle right) for facilitating neurons in central regions of IC under baseline and laser conditions. Change in firing rate between the laser and baseline condition for each stimulus (right). Dots represent individual neurons. Bar plots represent means over the population of n = 14 neurons. Error bars are standard error of the mean. D) Responses to the standard (left), cascade (middle left), and deviant (middle right) for facilitating neurons in shell regions of IC under baseline and laser conditions. Change in firing rate between the laser and baseline condition for each stimulus (right). Dots represent individual neurons. Bar plots represent means over the population of n = 38 neurons. Error bars are standard error of the mean. E) Responses to the standard (left), cascade (middle left), and deviant (middle right) for non-adapting neurons in central regions of IC under baseline and laser conditions. Change in firing rate between the laser and baseline condition for each stimulus (right). Dots represent individual neurons. Bar plots represent means over the population of n = 155 neurons. Error bars are standard error of the mean. F) Responses to the standard (left), cascade (middle left), and deviant (middle right) for non-adapting neurons in shell regions of IC under baseline and laser conditions. Change in firing rate between the laser and baseline condition for each stimulus (right). Dots represent individual neurons. Bar plots represent means over the population of n = 243 neurons. Error bars are standard error of the mean.

as well as a separate population exhibiting significant prediction error and repetition enhancement (Figure 8B, maroon dots). Some shell adapting neurons also exhibited a combination of both repetition suppression and prediction error (Figure 8B, left). These results suggest that individual neurons in IC exhibit distinct combinations of repetition suppression/enhancement and prediction error/error suppression.

Facilitating neurons exhibit true repetition enhancement

Facilitating neurons in both central and shell regions of IC exhibited repetition enhancement at baseline, as defined by the difference in firing rate to the last standard and the same tone embedded in the cascade sequence (Figure 5G, 5H). We sought to further characterize the response to the standard context to determine whether the repetition enhancement captured by the iRS indicates true repetition enhancement (an incremental increase in firing rate on subsequent presentations of the standard) or simply a net increase in firing rate to the standard versus cascade condition. We calculated the mean firing rate for each of the three standards before the deviant and each of the three standards after the deviant (Figure 8C, 8D). The progression of standards by position exhibited subsequent enhancements in firing rate that plateaued by the second to last standard before the deviant for both central (Figure 8C) and shell facilitating neurons (Figure 8D). The firing rate to the last standard was significantly higher than the first in both regions (Figure 8C, Table 1; $p=0.0017$, Wilcoxon signed rank test; Figure 8D, Table 1; $p=9.3e-05$, Wilcoxon signed rank test). These data provide evidence that facilitating neurons in IC exhibit true repetition enhancement.

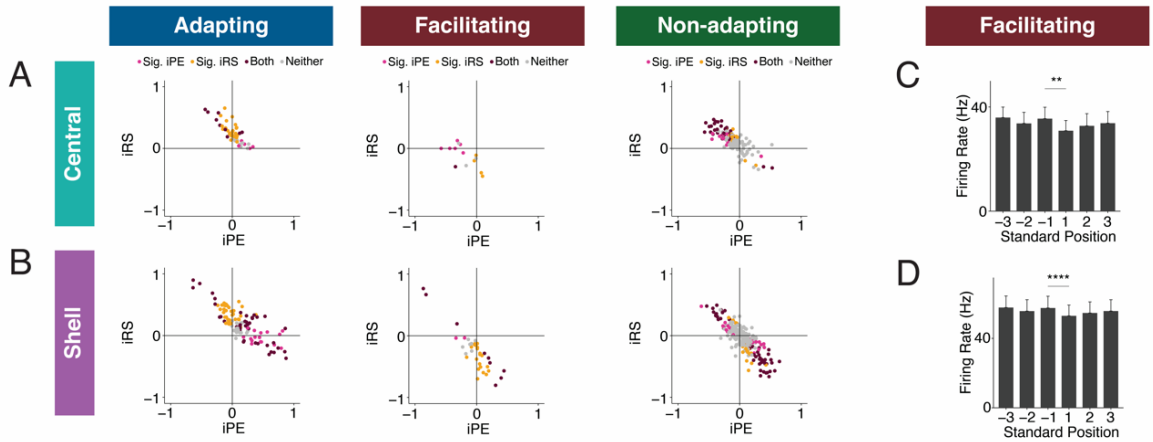

Figure 8: Individual neurons exhibit distinct combinations of iPE and iRS. A) Distribution of both iRS and iPE in individual adapting (left), facilitating (middle), and non-adapting (right) neurons in central IC. B) Plots of distributions of both iRS and iPE in individual adapting (left), facilitating (middle), and non-adapting (right) neurons in shell IC. C) Response to three subsequent standards prior to or following the deviant in facilitating neurons in central IC. Comparison between the last standard before and the first standard after the deviant demonstrates significant repetition enhancement. Bar plots represent means over the population of n = 14 neurons. Error bars are standard error of the mean. D) Response to three subsequent standards prior to or following the deviant in facilitating neurons in shell IC. Comparison between the last standard before and the first standard after the deviant demonstrates significant repetition enhancement. Bar plots represent means over the population of n = 38 neurons. Error bars are standard error of the mean.

604 DISCUSSION

605 *Summary of findings*

606 The results of the present study indicate that AC is critically involved in regulating both
607 repetition and prediction effects in the awake IC, providing evidence for the implementation of
608 predictive coding in cortico-subcortical networks. Adapting and facilitating neurons were bi-
609 directionally modulated by cortico-collicular suppression, with adapting neurons becoming less
610 adapting and facilitating neurons becoming less facilitating on laser trials (Figure 5). The decrease in
611 adaptation for adapting neurons was driven by a decrease in prediction error for neurons in both
612 central and shell regions of IC (Figure 5D, 5E). For facilitating neurons in the central nucleus,
613 suppression-driven changes were caused by a decrease in repetition enhancement (Figure 5G). The
614 decrease in facilitation in the shell IC, however, was caused by the abolishment of error suppression
615 (Figure 5H).

616 In adapting neurons, these changes were modulated by an increased response to the standard
617 and a decreased response to the deviant, while the opposite pattern was true for facilitating neurons
618 (Figure 7). Overall, these bi-directional changes indicate that, without input from AC, IC responds
619 more similarly to tones in the standard and deviant contexts. These findings demonstrate that AC
620 provides critical contextual cues about the statistics of the auditory environment to targets in IC under
621 normal conditions. We further discuss these results in the context of a hierarchical predictive coding
622 framework below.

623

624 *iMM in the awake versus anesthetized IC*

625 Our results include the first investigation of how the repetition and prediction processes that
626 underlie deviance detection in the awake IC compare to the anesthetized condition. Our data suggest
627 that while iMM values are higher under anesthesia, they almost entirely reflect repetition suppression,
628 with only a small contribution of prediction error (Figure 4). In the shell IC, the same neurons exhibit
629 drastically different iPE and iRS values for the awake versus the anesthetized condition. Prediction
630 error is substantially higher in the awake IC and repetition enhancement, rather than repetition
631 suppression, is observed (Figure 4F, 4G). These findings suggest that the iMM values in the awake
632 and anesthetized brain reflect different underlying processes, and that anesthesia induces bidirectional
633 changes in metrics of repetition and prediction.

634

635 *Facilitating neurons in IC*

We also provide here the first analysis of facilitating neurons in IC. Previous studies that have investigated iMM have focused selectively on the positive side of the iMM distribution, since these neurons display adaptation. However, facilitation seems to be enriched in the awake IC (Figure 4B, 4E) and reflects other potentially interesting parameters, such as repetition enhancement (represented as a higher response to the standard than the cascade sequence) (Figure 4G) and error suppression (represented as a higher response to the cascade than the deviant) (Figure 4C).

Repetition enhancement and repetition suppression in IC

Because previous studies that have applied a predictive coding framework to decompose neuronal mismatch have focused exclusively on adapting neurons, the repetition enhancement found here in facilitating neurons has not been previously described (Parras et al., 2017). However, it is well-documented in fMRI literature that repetition enhancement is a common phenomenon in humans, existing either alongside or in place of repetition suppression (De Gardelle et al., 2013; Müller et al., 2013; Segaert et al., 2013). Interestingly, repetition enhancement has been proposed to reflect novel network formation and consolidation of novel sensory representations (Segaert et al., 2013). Once new representations have been formed, repetition suppression is hypothesized to take over, reflecting the minimization in prediction errors that occurs when new representations give rise to accurate predictions (Auksztulewicz & Friston, 2016; De Gardelle et al., 2013; Friston & Kiebel, 2009). Though the repetition enhancement described in human studies differs drastically on spatial and temporal scales from the phenomenon described here, we find that it similarly involves a sequential enhancement in the response to subsequent presentations of the standard (Figure 8C, 8D).

While repetition suppression can be understood from a predictive coding framework, it can also be viewed from the perspective of neuronal fatigue, whereby the incremental decrease in firing rate to a repeated standard tone is simply explained by synaptic depression (Escera & Malmierca, 2014; Taaseh et al., 2011). Interestingly, we did not find any effect on repetition suppression during cortico-collicular suppression, suggesting that it may reflect fatigue of bottom-up sensory inputs rather than an active predictive process (Figure 5D, 5E). While these data do not provide definitive proof of either perspective, they do suggest that the processes that underlie repetition suppression in IC do not involve top-down cortical signals. This notion is supported by the fact that repetition suppression was much more prevalent when animals were under anesthesia, a state in which the auditory responsiveness in the cortex is compromised (Figure 4G) (Brugge & Merzenich, 1973; Katsuki et al., 1959).

Prediction error in IC

In both central and shell populations that exhibited prediction error at baseline, cortico-collicular suppression led to a decrease, or complete abolishment, of prediction error (Figure 5D, 5E). According to hierarchical predictive coding, higher-order stations generate predictions that they broadcast to lower centers (Friston & Kiebel, 2009). These predictions are compared with representations of the actual sensory input, and if there is a mismatch, a prediction error is generated and forwarded up the hierarchy (Friston & Kiebel, 2009). Under this framework, the suppression of top-down inputs would interfere with communication of predictions, leading to dysfunction in the prediction error response, as seen in our data. Another possibility is that prediction errors are directly backpropagated from AC to IC. While this contradicts canonical predictive coding models, evidence for prediction error has been found in deep layers of the cortex in which feedback neurons reside (Asilador & Llano, 2020; Rummell et al., 2016). Though the precise mechanism underlying the generation of prediction error in IC remains unclear, our data show that feedback from AC plays a critical role in this process.

Error suppression in IC

In addition to neurons with prediction error, we found neurons in IC that responded more strongly to the cascade than the deviant context (Figure 5G, 5H), consistent with previous reports (Parras et al., 2017). A stronger response to a tone in the cascade sequence compared to the context in which it is a deviant could simply reflect a relative lack of cross-frequency adaptation; the oddball stimulus consists of repeated tone presentations of two neighboring frequencies, making it more likely to generate cross-frequency effects than the cascade stimulus, which cycles through repetitions of 10 evenly-spaced frequencies (Parras et al., 2017; Taaseh et al., 2011). Previous studies that have investigated the effective bandwidth for cross-frequency adaptation, however, have found that it occurs between channels with a frequency separation of a third of an octave or less (Taaseh et al., 2011). The stimuli used in the present study had a half-octave frequency separation, indicating that cross-frequency effects should be minimized. Therefore, it is unlikely that the error suppression responses observed in the present study simply reflect cross-frequency adaptation to the oddball stimulus.

A stronger response to a tone when it is embedded in a completely predictable sequence, such as the cascade sequence, than when it is a deviant could also signify that a neuron encodes predictions, rather than prediction errors. In hierarchical predictive coding, both predictions and prediction errors are generated at every level of the hierarchy, with prediction errors being forwarded to ascending

sensory centers and predictions being backpropagated (Friston & Kiebel, 2009). In the shell IC, the region which receives the vast majority of descending cortical input, evidence for error suppression was abolished during cortico-collicular suppression (Figure 5H), consistent with the notion that feedback from the cortex may carry predictions to IC (Bajo et al., 2007; Herbert et al., 1991; Saldaña et al., 1996; Stebbings et al., 2014). Interestingly, error suppression in the central nucleus remained unperturbed during suppression of cortical feedback (Figure 5G). Given that only a small fraction of cortico-collicular fibers terminate in the central nucleus, it is likely that it receives predictions from another source (Bajo et al., 2007; Herbert et al., 1991; Saldaña et al., 1996; Stebbings et al., 2014). An intriguing potential candidate for this source of predictions could be the shell IC, given the extensive network of intracollicular connections in IC (Lesicko & Llano, 2020; Saldaña & Merchań, 1992; Saldaña & Merchán, 2005). Future studies will be required to determine whether the error suppression metric described here captures the type of top-down predictions described in canonical predictive coding models.

Technical considerations

One limitation of the present study is that laser photo-suppression achieved only partial suppression, and not complete inactivation, of the cortico-collicular pathway. Given that light itself can have a modulatory or toxic effect on neurons, these types of optogenetic experiments require a careful titration between using enough power to substantially affect the population of interest without causing non-specific light or heat-based perturbations (Tyssowski & Gray, 2019). Though other techniques, such as chemogenetic approaches or cooling, provide more complete suppression, they do not allow for rapid and reversible inactivation (English & Roth, 2015). With our laser power parameters, we found a mean 60% reduction in firing in putative cortico-collicular neurons at baseline and a 45% reduction during presentation of pure tone stimuli (Figure 2D). This reduction produced clear effects on repetition and prediction processing in IC, in several cases with the severe reduction or complete abolishment of certain metrics of deviance detection, such as prediction error and repetition enhancement in the central nucleus and error suppression in the shell IC (Figure 5). The interpretation of these results should bear in mind that they reflect only partial suppression and not complete inactivation.

Conclusions

Our findings indicate that deviance detection and predictive coding in IC involves additional complexity than has been previously described. We provide here the first description of facilitating

neurons in IC, as well as evidence for the existence of repetition enhancement and error suppression in these neurons. We show that AC regulates these metrics and is also involved in the generation of prediction error in IC. Repetition suppression is unaffected by suppression of cortical input to IC, providing evidence that this process may reflect bottom-up fatigue rather than top-down predictive processing. These results demonstrate the role of AC in providing contextual cues about the auditory stream to targets in IC.

Acknowledgements

The authors thank members of the Geffen laboratory for helpful discussions. This work was supported by funding from the National Institute of Health grants F32MH120890 to AMHL, R01DC015527, R01DC014479 and R01NS113241 to MNG, F31DC016524 to CA, and R01DA044205, R01DA049545 and U01AA025931 to MDB.

747 Table 1: Statistical comparisons for experimental data.

Comparison	Figure	Test	Test statistic	N	df	p
Response of putative cortico-collicular neurons in silence (laser ON vs. OFF)	2D (top)	Wilcoxon signed rank test	V = 0	20	NA	1.91e-06
Response of putative cortico-collicular neurons to pure tones (laser ON vs. OFF)	2D (bottom)	Wilcoxon signed rank test	V = 0	20	NA	1.91e-06
iMM central (awake vs. anesthetized)	4B	Paired t-test	t = -2.1	39	38	0.039
iPE central (awake vs. anesthetized)	4C	Paired t-test	t = -2.0	39	38	0.056
iRS central (awake vs. anesthetized)	4D	Wilcoxon signed rank test	V = 331	39	NA	0.42
iMM shell (awake vs. anesthetized)	4E	Wilcoxon signed rank test	V = 3317	165	NA	1.51e-08
iPE shell (awake vs. anesthetized)	4F	Wilcoxon signed rank test	V = 9455	165	NA	2.2e-05
iRS shell (awake vs. anesthetized)	4G	Wilcoxon signed rank test	V = 2150	165	NA	2.1e-14
iMM central adapting (laser ON vs. OFF)	5D (top)	Wilcoxon signed rank test	V = 1083	52	NA	0.00034
iPE central adapting (laser ON vs. OFF)	5D (middle)	Wilcoxon signed rank test	V = 907	52	NA	0.048
iRS central adapting (laser ON vs. OFF)	5D (bottom)	Wilcoxon signed rank test	V = 832	52	NA	0.19
iMM shell adapting (laser ON vs. OFF)	5E (top)	Wilcoxon signed rank test	V = 4283	113	NA	0.0023
iPE shell adapting (laser ON vs. OFF)	5E (middle)	Wilcoxon signed rank test	V = 3963	113	NA	0.034
iRS shell adapting (laser ON vs. OFF)	5E (bottom)	Paired t-test	t = 1.6	113	112	0.11
iMM central facilitating (laser ON vs. OFF)	5G (top)	Paired t-test	t = -3.5	14	13	0.0036
iPE central facilitating (laser ON vs. OFF)	5G (middle)	Paired t-test	t = -1.2	14	13	0.25
iRS central facilitating (laser ON vs. OFF)	5G (bottom)	Paired t-test	t = -3.7	14	13	0.0026
iMM shell facilitating (laser ON vs. OFF)	5H (top)	Wilcoxon signed rank test	V = 159	38	NA	0.0016
iPE shell facilitating (laser ON vs. OFF)	5H (middle)	Wilcoxon signed rank test	V = 227	38	NA	0.037
iRS shell facilitating (laser ON vs. OFF)	5H (bottom)	Wilcoxon signed rank test	V = 254	38	NA	0.093
iMM central non-adapting (laser ON vs. OFF)	6C (top)	Wilcoxon signed rank test	V = 3419	155	NA	2.7e-06

iPE central non-adapting (laser ON vs. OFF)	6C (middle)	Wilcoxon signed rank test	V = 5327	155	NA	0.20
iRS central non-adapting (laser ON vs. OFF)	6C (bottom)	Wilcoxon signed rank test	V = 4224	155	NA	0.0011
iMM shell non-adapting (laser ON vs. OFF)	6D (top)	Wilcoxon signed rank test	V = 12765	243	NA	0.076
iPE shell non-adapting (laser ON vs. OFF)	6D (middle)	Wilcoxon signed rank test	V = 13474	243	NA	0.22
iRS shell non-adapting (laser ON vs. OFF)	6D (bottom)	Wilcoxon signed rank test	V = 14344	243	NA	0.66
FR standard central adapting (laser ON vs. OFF)	7A	Wilcoxon signed rank test	V = 378.5	52	NA	0.020
FR cascade central adapting (laser ON vs. OFF)	7A	Wilcoxon signed rank test	V = 692	52	NA	0.79
FR deviant central adapting (laser ON vs. OFF)	7A	Wilcoxon signed rank test	V = 972.5	52	NA	0.0038
FR standard shell adapting (laser ON vs. OFF)	7B	Wilcoxon signed rank test	V = 2345	113	NA	0.035
FR cascade shell adapting (laser ON vs. OFF)	7B	Wilcoxon signed rank test	V = 2888	113	NA	0.62
FR deviant shell adapting (laser ON vs. OFF)	7B	Wilcoxon signed rank test	V = 3846	113	NA	0.0057
FR standard central facilitating (laser ON vs. OFF)	7C	Wilcoxon signed rank test	V = 97	14	NA	0.0057
FR cascade central facilitating (laser ON vs. OFF)	7C	Wilcoxon signed rank test	V = 57	14	NA	0.80
FR deviant central facilitating (laser ON vs. OFF)	7C	Wilcoxon signed rank test	V = 25.5	14	NA	0.096
FR standard shell facilitating (laser ON vs. OFF)	7D	Wilcoxon signed rank test	V = 562.5	38	NA	0.0055
FR cascade shell facilitating (laser ON vs. OFF)	7D	Wilcoxon signed rank test	V = 318	38	NA	0.82
FR deviant shell facilitating (laser ON vs. OFF)	7D	Wilcoxon signed rank test	V = 159.5	38	NA	0.0023
FR standard central non-adapting (laser ON vs. OFF)	7E	Wilcoxon signed rank test	V = 8031	155	NA	1.4e-06
FR cascade central non-adapting (laser ON vs. OFF)	7E	Wilcoxon signed rank test	V = 6084.5	155	NA	0.16
FR deviant central non-adapting (laser ON vs. OFF)	7E	Wilcoxon signed rank test	V = 5027.5	155	NA	0.29
FR standard shell non-adapting (laser ON vs. OFF)	7F	Wilcoxon signed rank test	V = 15284	243	NA	0.035
FR cascade shell non-adapting (laser ON vs. OFF)	7F	Wilcoxon signed rank test	V = 15104	243	NA	0.15
FR deviant shell non-adapting (laser ON vs. OFF)	7F	Wilcoxon signed rank test	V = 14022	243	NA	0.88
FR central facilitating (first vs. last standard)	8C	Wilcoxon signed rank test	V = 0	14	NA	0.0017

FR shell facilitating (first vs. last standard)	8D	Wilcoxon signed rank test	V = 92	38	NA	9.3e-05
FR central adapting (cascade vs. many standards)	S2B (left)	Wilcoxon signed rank test	V = 595	52	NA	0.39
FR central facilitating (cascade vs. many standards)	S2B (right)	Wilcoxon signed rank test	V = 41	14	NA	0.49
FR shell adapting (cascade vs. many standards)	S2C (left)	Wilcoxon signed rank test	V = 2653	113	NA	0.46
FR shell facilitating (cascade vs. many standards)	S2C (right)	Wilcoxon signed rank test	V = 264.5	38	NA	0.41

Table 2: Statistical comparisons for control data.

Comparison	**Figure**	**Test**	**Test statistic**	**N**	**df**	**p**
iMM central (control vs. experimental)	S1B (left)	Wilcoxon rank sum test	W = 7919	77 (control) 221 (exp.)	NA	0.37
iMM shell (control vs. experimental)	S1B (right)	Wilcoxon rank sum test	W = 22364	119 (control) 394 (exp.)	NA	0.45
iMM central adapting (laser ON vs. OFF)	S1C (top)	Wilcoxon signed rank test	V = 124	18	NA	0.099
iPE central adapting (laser ON vs. OFF)	S1C (middle)	Paired t-test	t = -1.1	18	17	0.30
iRS central adapting (laser ON vs. OFF)	S1C (bottom)	Paired t-test	t = 1.9	18	17	0.077
iMM shell adapting (laser ON vs. OFF)	S1D (top)	Paired t-test	t = -0.0013	35	34	0.99
iPE shell adapting (laser ON vs. OFF)	S1D (middle)	Paired t-test	t = 0.58	35	34	0.56
iRS shell adapting (laser ON vs. OFF)	S1D (bottom)	Paired t-test	t = -0.78	35	34	0.44
iMM central facilitating (laser ON vs. OFF)	S1E (top)	Paired t-test	t = -1.1	4	3	0.34
iPE central facilitating (laser ON vs. OFF)	S1E (middle)	Paired t-test	t = -0.93	4	3	0.42
iRS central facilitating (laser ON vs. OFF)	S1E (bottom)	Paired t-test	t = 0.49	4	3	0.66
iMM shell facilitating (laser ON vs. OFF)	S1F (top)	Wilcoxon signed rank test	V = 63	21	NA	0.070
iPE shell facilitating (laser ON vs. OFF)	S1F (middle)	Wilcoxon signed rank test	V = 109	21	NA	0.84
iRS shell facilitating (laser ON vs. OFF)	S1F (bottom)	Paired t-test	t = -1.8	21	20	0.091
iMM central non-adapting (laser ON vs. OFF)	S1G (top)	Paired t-test	t = -1.8	55	54	0.075
iPE central non-adapting (laser ON vs. OFF)	S1G (middle)	Paired t-test	t = -1.2	55	54	0.23
iRS central non-adapting (laser ON vs. OFF)	S1G (bottom)	Paired t-test	t = -0.57	55	54	0.57

iMM shell non-adapting (laser ON vs. OFF)	S1H (top)	Wilcoxon signed rank test	V = 1133	63	NA	0.39
iPE shell non-adapting (laser ON vs. OFF)	S1H (middle)	Paired t-test	t = 0.88	63	62	0.38
iRS shell non-adapting (laser ON vs. OFF)	S1H (bottom)	Paired t-test	t = -0.43	63	62	0.67

REFERENCES

Aitkin, L. M., Webster, W. R., Veale, J. L., & Crosby, D. C. (1975). Inferior colliculus. I. Comparison of response properties of neurons in central, pericentral, and external nuclei of adult cat. *Journal of Neurophysiology*, *38*(5), 1196–1207.

Anderson, L A, & Malmierca, M. S. (2013). The effect of auditory cortex deactivation on stimulus-specific adaptation in the inferior colliculus of the rat. *European Journal of Neuroscience*, *37*(1), 52–62.

Anderson, Lucy A, Christianson, G. B., & Linden, J. F. (2009). Stimulus-specific adaptation occurs in the auditory thalamus. *Journal of Neuroscience*, *29*(22), 7359–7363.

Antunes, F. M., & Malmierca, M. S. (2011). Effect of auditory cortex deactivation on stimulus-specific adaptation in the medial geniculate body. *Journal of Neuroscience*, *31*(47), 17306–17316.

Antunes, F. M., Nelken, I., Covey, E., & Malmierca, M. S. (2010). Stimulus-specific adaptation in the auditory thalamus of the anesthetized rat. *PLoS One*, *5*(11), e14071.

Asilador, A., & Llano, D. A. (2020). Top-down inference in the auditory system: Potential roles for corticofugal projections. *Frontiers in Neural Circuits*, *14*.

Auksztulewicz, R., & Friston, K. (2016). Repetition suppression and its contextual determinants in predictive coding. *Cortex*, *80*, 125–140.

Bajo, V. M., Nodal, F. R., Bizley, J. K., Moore, D. R., & King, A. J. (2007). The ferret auditory cortex: descending projections to the inferior colliculus. *Cerebral Cortex*, *17*(2), 475–491.

Bastos, A. M., Usrey, W. M., Adams, R. A., Mangun, G. R., Fries, P., & Friston, K. J. (2012). Canonical microcircuits for predictive coding. *Neuron*, *76*(4), 695–711.

Blackwell, J. M., Lesicko, A., Rao, W., De Biasi, M., & Geffen, M. N. (2020). Auditory cortex shapes sound responses in the inferior colliculus. *ELife*, *9*. https://doi.org/10.7554/eLife.51890

Brugge, J. F., & Merzenich, M. M. (1973). Responses of neurons in auditory cortex of the macaque monkey to monaural and binaural stimulation. *Journal of Neurophysiology*, *36*(6), 1138–1158.

Chen, C., Rodriguez, F. C., Read, H., & Escabí, M. A. (2012). Spectrotemporal sound preferences of neighboring inferior colliculus neurons: implications for local circuitry and processing. *Frontiers in Neural Circuits*, *6*, 62.

De Franceschi, G., & Barkat, T. R. (2020). Task-induced modulations of neuronal activity along the auditory pathway. *BioRxiv*.

De Gardelle, V., Waszczuk, M., Egner, T., & Summerfield, C. (2013). Concurrent repetition enhancement and suppression responses in extrastriate visual cortex. *Cerebral Cortex*, *23*(9),

2235–2244.

Duque, D., & Malmierca, M. S. (2015). Stimulus-specific adaptation in the inferior colliculus of the mouse: anesthesia and spontaneous activity effects. *Brain Structure and Function*, *220*(6), 3385–3398.

Duque, D., Pérez-González, D., Ayala, Y. A., Palmer, A. R., & Malmierca, M. S. (2012). Topographic distribution, frequency, and intensity dependence of stimulus-specific adaptation in the inferior colliculus of the rat. *Journal of Neuroscience*, *32*(49), 17762–17774.

English, J. G., & Roth, B. L. (2015). Chemogenetics—a transformational and translational platform. *JAMA Neurology*, *72*(11), 1361–1366.

Escera, C., & Malmierca, M. S. (2014). The auditory novelty system: an attempt to integrate human and animal research. *Psychophysiology*, *51*(2), 111–123.

Fontanini, A., & Katz, D. B. (2008). Behavioral states, network states, and sensory response variability. *Journal of Neurophysiology*, *100*(3), 1160–1168.

Friston, K. (2009). The free-energy principle: a rough guide to the brain? *Trends in Cognitive Sciences*, *13*(7), 293–301.

Friston, K., & Kiebel, S. (2009). Predictive coding under the free-energy principle. *Philosophical Transactions of the Royal Society B: Biological Sciences*, *364*(1521), 1211–1221.

Gaese, B. H., & Ostwald, J. (2001). Anesthesia changes frequency tuning of neurons in the rat primary auditory cortex. *Journal of Neurophysiology*, *86*(2), 1062–1066.

Han, X., Chow, B. Y., Zhou, H., Klapoetke, N. C., Chuong, A., Rajimehr, R., Yang, A., Baratta, M. V, Winkle, J., & Desimone, R. (2011). A high-light sensitivity optical neural silencer: development and application to optogenetic control of non-human primate cortex. *Frontiers in Systems Neuroscience*, *5*, 18.

Harms, L., Fulham, W. R., Todd, J., Budd, T. W., Hunter, M., Meehan, C., Penttonen, M., Schall, U., Zavitsanou, K., & Hodgson, D. M. (2014). Mismatch negativity (MMN) in freely-moving rats with several experimental controls. *PloS One*, *9*(10), e110892.

Herbert, H., Aschoff, A., & Ostwald, J. (1991). Topography of projections from the auditory cortex to the inferior colliculus in the rat. *Journal of Comparative Neurology*, *304*(1), 103–122.

Herrmann, B., Henry, M. J., Fromboluti, E. K., McAuley, J. D., & Obleser, J. (2015). Statistical context shapes stimulus-specific adaptation in human auditory cortex. *Journal of Neurophysiology*, *113*(7), 2582–2591.

Jaramillo, S., Borges, K., & Zador, A. M. (2014). Auditory thalamus and auditory cortex are equally modulated by context during flexible categorization of sounds. *Journal of Neuroscience*,

34(15), 5291–5301.

Johnson, K. R., Tian, C., Gagnon, L. H., Jiang, H., Ding, D., & Salvi, R. (2017). Effects of Cdh23 single nucleotide substitutions on age-related hearing loss in C57BL/6 and 129S1/Sv mice and comparisons with congenic strains. *Scientific Reports*, *7*(1), 1–13.

Katsuki Y., Murata, K., Suga, N., & Takenaka, T. (1959). Electrical activity of cortical auditory neurons of unanaesthetized and unrestrained cat. *Proceedings of the Japan Academy*, *35*(9), 571–574.

Lesicko, A.M.H., Hristova, T. S., Maigler, K. C., & Llano, D. A. (2016). Connectional modularity of top-down and bottom-up multimodal inputs to the lateral cortex of the mouse inferior colliculus. *Journal of Neuroscience*, *36*(43). https://doi.org/10.1523/JNEUROSCI.4134-15.2016

Lesicko, Alexandria M H, & Llano, D. A. (2020). Circuit mechanisms underlying the segregation and integration of parallel processing streams in the inferior colliculus. *Journal of Neuroscience*, *40*(33), 6328–6344.

Malmierca, M. S., Cristaudo, S., Pérez-González, D., & Covey, E. (2009). Stimulus-specific adaptation in the inferior colliculus of the anesthetized rat. *Journal of Neuroscience*, *29*(17), 5483–5493.

Malmierca, M. S., Izquierdo, M. A., Cristaudo, S., Hernández, O., Pérez-González, D., Covey, E., & Oliver, D. L. (2008). A discontinuous tonotopic organization in the inferior colliculus of the rat. *Journal of Neuroscience*, *28*(18), 4767–4776.

Müller, N. G., Strumpf, H., Scholz, M., Baier, B., & Melloni, L. (2013). Repetition suppression versus enhancement—it's quantity that matters. *Cerebral Cortex*, *23*(2), 315–322.

Natan, R. G., Briguglio, J. J., Mwilambwe-Tshilobo, L., Jones, S. I., Aizenberg, M., Goldberg, E. M., & Geffen, M. N. (2015). Complementary control of sensory adaptation by two types of cortical interneurons. *Elife*, *4*, e09868.

Nelken, I., & Ulanovsky, N. (2007). Mismatch negativity and stimulus-specific adaptation in animal models. *Journal of Psychophysiology*, *21*(3–4), 214–223.

Okada, K., Matchin, W., & Hickok, G. (2018). Neural evidence for predictive coding in auditory cortex during speech production. *Psychonomic Bulletin & Review*, *25*(1), 423–430.

Pakan, J. M. P., Lowe, S. C., Dylda, E., Keemink, S. W., Currie, S. P., Coutts, C. A., & Rochefort, N. L. (2016). Behavioral-state modulation of inhibition is context-dependent and cell type specific in mouse visual cortex. *Elife*, *5*, e14985.

Parras, G. G., Nieto-Diego, J., Carbajal, G. V, Valdés-Baizabal, C., Escera, C., & Malmierca, M. S.

(2017). Neurons along the auditory pathway exhibit a hierarchical organization of prediction error. *Nature Communications*, *8*(1), 1–17.

Rao, R. P. N., & Ballard, D. H. (1999). Predictive coding in the visual cortex: a functional interpretation of some extra-classical receptive-field effects. *Nature Neuroscience*, *2*(1), 79–87.

Rauss, K., Schwartz, S., & Pourtois, G. (2011). Top-down effects on early visual processing in humans: A predictive coding framework. *Neuroscience & Biobehavioral Reviews*, *35*(5), 1237–1253.

Ruhnau, P., Herrmann, B., & Schröger, E. (2012). Finding the right control: the mismatch negativity under investigation. *Clinical Neurophysiology*, *123*(3), 507–512.

Rummell, B. P., Klee, J. L., & Sigurdsson, T. (2016). Attenuation of responses to self-generated sounds in auditory cortical neurons. *Journal of Neuroscience*, *36*(47), 12010–12026.

Saldaña, E., Feliciano, M., & Mugnaini, E. (1996). Distribution of descending projections from primary auditory neocortex to inferior colliculus mimics the topography of intracollicular projections. *Journal of Comparative Neurology*, *371*(1), 15–40.

Saldaña, E., & Merchań, M. A. (1992). Intrinsic and commissural connections of the rat inferior colliculus. *Journal of Comparative Neurology*, *319*(3), 417–437.

Saldaña, E., & Merchán, M. A. (2005). Intrinsic and commissural connections of the inferior colliculus. In *The inferior colliculus* (pp. 155–181). Springer.

Schellekens, W., Van Wezel, R. J. A., Petridou, N., Ramsey, N. F., & Raemaekers, M. (2016). Predictive coding for motion stimuli in human early visual cortex. *Brain Structure and Function*, *221*(2), 879–890.

Schofield, B. R. (2009). Projections to the inferior colliculus from layer VI cells of auditory cortex. *Neuroscience*, *159*(1), 246–258.

Schumacher, J. W., Schneider, D. M., & Woolley, S. M. N. (2011). Anesthetic state modulates excitability but not spectral tuning or neural discrimination in single auditory midbrain neurons. *Journal of Neurophysiology*, *106*(2), 500–514.

Segaert, K., Weber, K., de Lange, F. P., Petersson, K. M., & Hagoort, P. (2013). The suppression of repetition enhancement: a review of fMRI studies. *Neuropsychologia*, *51*(1), 59–66.

Shipp, S. (2016). Neural elements for predictive coding. *Frontiers in Psychology*, *7*, 1792.

Shipp, S., Adams, R. A., & Friston, K. J. (2013). Reflections on agranular architecture: predictive coding in the motor cortex. *Trends in Neurosciences*, *36*(12), 706–716.

Stebbings, K. A., Lesicko, A. M. H., & Llano, D. A. (2014). The auditory corticocollicular system: Molecular and circuit-level considerations. *Hearing Research*, *314*.

https://doi.org/10.1016/j.heares.2014.05.004

Stiebler, I., & Ehret, G. (1985). Inferior colliculus of the house mouse. I. A quantitative study of tonotopic organization, frequency representation, and tone-threshold distribution. *Journal of Comparative Neurology*, *238*(1), 65–76.

Syka, J., Popelář, J., Kvašňák, E., & Astl, J. (2000). Response properties of neurons in the central nucleus and external and dorsal cortices of the inferior colliculus in guinea pig. *Experimental Brain Research*, *133*(2), 254–266.

Taaseh, N., Yaron, A., & Nelken, I. (2011). Stimulus-specific adaptation and deviance detection in the rat auditory cortex. *PloS One*, *6*(8), e23369.

Takesian, A. E., Bogart, L. J., Lichtman, J. W., & Hensch, T. K. (2018). Inhibitory circuit gating of auditory critical-period plasticity. *Nature Neuroscience*, *21*(2), 218–227.

Torii, M., Hackett, T. A., Rakic, P., Levitt, P., & Polley, D. B. (2013). EphA signaling impacts development of topographic connectivity in auditory corticofugal systems. *Cerebral Cortex*, *23*(4), 775–785.

Tyssowski, K. M., & Gray, J. M. (2019). Blue light increases neuronal activity-regulated gene expression in the absence of optogenetic proteins. *ENeuro*, *6*(5).

Ulanovsky, N., Las, L., & Nelken, I. (2003). Processing of low-probability sounds by cortical neurons. *Nature Neuroscience*, *6*(4), 391–398.

Weissbart, H., Kandylaki, K. D., & Reichenbach, T. (2020). Cortical tracking of surprisal during continuous speech comprehension. *Journal of Cognitive Neuroscience*, *32*(1), 155–166.

Yaron, A., Hershenhoren, I., & Nelken, I. (2012). Sensitivity to complex statistical regularities in rat auditory cortex. *Neuron*, *76*(3), 603–615.

Yudintsev, G., Asilador, A., Coppinger, M., Nair, K., Prasad, M., & Llano, D. A. (2019). Connectional heterogeneity in the mouse auditory corticocollicular system. *BioRxiv*, 571711.

Zhai, X., Khatami, F., Sadeghi, M., He, F., Read, H. L., Stevenson, I. H., & Escabí, M. A. (2020). Distinct neural ensemble response statistics are associated with recognition and discrimination of natural sound textures. *Proceedings of the National Academy of Sciences*, *117*(49), 31482–31493.